electronics

MDPI

Article

Cross-Order Distortion Descriptor (CDD) for Paired Voltage and Current Harmonic Spectra: Separating THD-Determined and Order-Dependent Parts

Daniel D. Campo-Ossa [1,*], G. Alejandra Feo-Cediel [2] and Fabio Andrade Rengifo [2,*]

[1] Technology and Applied Sciences Department, University of Puerto Rico at Aguadilla, Aguadilla, PR 00604, USA
[2] Electrical and Computer Engineering Department, University of Puerto Rico at Mayagüez, Mayagüez, PR 00682, USA; guisellealejandra.feo@upr.edu
* Correspondence: daniel.campo@upr.edu (D.D.C.-O.); fabio.andrade@upr.edu (F.A.R.)

Abstract

In power-quality studies of power electronic converters, total harmonic distortion (THD) summarizes voltage and current spectra separately, obscuring their joint organization across harmonic orders. We develop the Cross-Order Distortion Descriptor (CDD), a magnitude-only descriptor of paired per-order root-mean-square (RMS) voltage and current spectra. In its exact factorization, the fundamental-related part is fixed by the fundamental RMS product and the two THD values, whereas the harmonic–harmonic part additionally depends on $\kappa \in [0, 1]$, the complement of the normalized same-order spectral overlap, which approximately locates a record below the THD-imposed ceiling. In the pair with the largest separation in κ among 2500 simulated diode-bridge rectifier supply spectra with equal voltage THD and nearly equal current THD, $\kappa = 0.96$ and 0.34 accompany different conduction intervals; reversing the third-harmonic phase, with voltage magnitudes unchanged, reverses that ordering. In induction-motor records, the harmonic–harmonic part of CDD rises by 11.8% through κ at a nearly unchanged scale under illustrative error scenarios, whereas photovoltaic-inverter tests approximately double both THD values at nearly constant κ. In capacitor records, κ nearly follows joint spectral concentration; in data-center and capacitor records, harmonic–harmonic contributions stay small at low voltage THD, as the bounds require. CDD characterizes paired harmonic spectra, separating THD-determined and order-dependent contributions.

Keywords: cross-order distortion descriptor; total harmonic distortion; harmonic spectra; power electronic converters; diode-bridge rectifier; power quality; IEEE Std 1459

Check for updates

Academic Editor: Kan Akatsu

Received: 11 October 2026
Revised: 30 October 2026
Accepted: 2 November 2026
Published: 4 November 2026

Copyright: © 2026 by the authors. Licensee MDPI, Basel, Switzerland. This article is an open access article distributed under the terms and conditions of the Creative Commons Attribution (CC BY) license.

1. Introduction

Many power-quality analyzers report per-order root-mean-square (RMS) magnitudes of voltage and current over a common observation interval, and they commonly summarize each spectrum by its total harmonic distortion (THD): voltage THD and current THD. For compliance assessment at the point of common coupling, IEEE Std 519-2022 uses voltage THD and current total demand distortion (TDD), whereas IEC 61000-4-7 specifies how the underlying harmonic components are measured [1,2]. In this paper, current THD is used as a spectral summary normalized by the fundamental, not as a compliance index. Harmonic limits and engineering studies distinguish aggregate THD from individual harmonic components [3,4]. For rectifiers and other nonlinear loads, the order-resolved

spectrum is the working quantity in engineering practice: a balanced six-pulse converter exhibits characteristic current harmonics at orders $6k \pm 1$, passive filters are tuned to specific orders, and a parallel resonance can amplify harmonic components near its resonant frequency; none of these order-specific features can be inferred from a THD value alone [4,5]. Interconnection standards for distributed and inverter-based resources, such as grid-tied photovoltaic and wind generation, likewise use individual-order limits and an aggregate limit, total rated-current distortion (TRD), at declared reference points, and recognize that the measured harmonic current depends on background voltage distortion [6,7]. Because the harmonic current emission of power electronic converters and other nonlinear loads depends on the supply voltage distortion [8], converter modeling, simulation, and power-quality assessment deal with paired voltage and current spectra.

These limits and summaries, however, evaluate each spectrum, or each order, separately; they do not describe how the voltage and current spectra are organized relative to each other across orders. When a record archives only the fundamental components and the two THD values, this pairing of voltage and current content across harmonic orders is lost. Established tools answer different questions: THD quantifies the distortion of each spectrum; IEEE Std 1459 defines how power and RMS quantities are measured under nonsinusoidal conditions and places THD, a power-quality quantity, outside its scope (Annex G) [9]; and instantaneous power theory represents power in the time domain for analysis and control [10,11]. This paper addresses a different and narrower question: given one paired voltage–current magnitude spectrum, which part of its joint order-by-order organization is already implied by the two THD values, and which part is not? Here, order-by-order organization refers to how the nonfundamental RMS content of the voltage and current spectra is distributed among harmonic orders and how those distributions overlap at the same orders.

Products of voltage and current at different harmonic orders are well established in phase-resolved analyses of nonsinusoidal power and harmonic power flow [12–14], including current decompositions such as the physical components of currents and the conservative power theory [15,16]. Physical cross-frequency behavior is modeled by phase-resolved input–output formulations, including experimentally identified crossed-frequency admittances [17], converter frequency-coupling matrices [18,19], and related formulations for AC/DC converters and voltage-dependent loads [20,21] and for inverter-based resources [22]; harmonic state-space and impedance-based methods address dynamic and network objectives [23,24]. In such input–output formulations, off-diagonal terms can represent cross-frequency transfer or coupling relationships.

Matrix and tensor representations of voltage–current products have established precedents: tensor and geometric-algebra formulations represent power through products of voltage and current components [25,26], and LaWhite and Ilić expressed Fryze's reactive power as the Frobenius norm of an antisymmetric matrix of cross products of Fourier coefficients [27]. Those constructions retain phase and address power definitions. Hartman and Hashad [28] used the square root of the off-diagonal quadratic sum $\sum_{m \neq n} V_m^2 I_n^2$ of harmonic RMS magnitudes as an apparent-power term within a power-theory formulation. Products of voltage and current magnitudes of different orders also appeared in the distortion-power definitions of IEEE Std 1459-2010 [29], which IEEE Std 1459-2025 omits (Annex G) [9]. The Cross-Order Distortion Descriptor (CDD) developed here applies the off-diagonal quadratic sum of paired harmonic RMS magnitudes as a spectral descriptor; it is not derived from the distortion-power definitions of IEEE Std 1459-2010 and carries no physical power interpretation.

This paper organizes the products $V_m I_n$ $(m \neq n)$ of paired per-order RMS magnitudes as the off-diagonal part of the outer product of paired magnitude spectra over a declared

set and derives an exact fundamental-related/harmonic–harmonic partition and its factorization in terms of the fundamental product, the two THD values, and one harmonic-order factor. The factorization yields closed-form THD bounds, and the resulting quantities are evaluated on simulated, published, and measured records. CDD is computed directly from the paired per-order magnitudes; the two THD values do not enter its definition but appear in its factorization, where they identify which terms aggregate distortion fixes and which require order-resolved information. In practice, records that archive only the fundamentals and the two THD values determine the fundamental-related part of CDD exactly, but not its harmonic–harmonic part, which requires the per-order spectra. Here, *cross-order* refers only to the index pairs (m, n), $m \neq n$, of the paired magnitude spectra. CDD is a *descriptor* of the observed paired spectral state; it is distinct from cross-order *coupling* or *response*, which phase-resolved input–output models identify from controlled variations [17,18,21]. Aggregate indices reduce the voltage and current spectra separately, whereas phase-aware power theories and frequency-coupled models retain substantially richer physical information; the present work addresses the case in which paired per-order RMS magnitudes are available, but harmonic phases or perturbation-based physical models are not.

The contributions are as follows:

1. An exact factorization of the cross-order products of paired per-order RMS magnitudes that separates the THD-determined and order-dependent parts of CDD, expresses the latter through the normalized harmonic-order factor κ, and yields closed-form THD bounds; κ approximates the normalized position of a record below its THD-imposed ceiling with an absolute error of at most $\min(a, b)^2/4$;
2. Evidence that distortion scale and normalized harmonic-order organization can change separately: in a published PV-inverter test, both THD values approximately double at nearly constant κ, whereas in a published induction-motor dataset the harmonic–harmonic scale $V_{H'} I_{H'}$ changes by 0.32%, a change not distinguishable from zero under illustrative error scenarios, while CDD_{HH} increases by 11.79% through κ; a hand-worked measured example and a simulated diode-bridge rectifier pair with matched voltage THD, selected reproducibly from a population of 2500 supply spectra, illustrate the reading;
3. A quantitative characterization of the regimes in which the harmonic–harmonic contribution is constrained to remain small: the THD bounds keep the harmonic–harmonic fraction $\eta_{HH} = \mathrm{CDD}_{HH}^2/\mathrm{CDD}^2$ below 0.64% whenever voltage THD is at most 8%, consistent with the small harmonic–harmonic contributions of the data-center and capacitor records; a controlled-injection test further shows that a physical cross-order response need not produce large CDD scalars; and
4. A comparison of κ with simpler order-resolved summaries of the same spectra, which identifies the same-order alignment that κ carries beyond single-spectrum concentration in the motor records and shows that its incremental descriptive value is dataset-dependent.

2. Materials and Methods

Sections 2.1 and 2.2 define CDD for one paired voltage–current magnitude spectrum and derive its exact relation to voltage and current THD; the results of Section 3 apply these definitions to constructed, simulated, published, and measured records.

2.1. CDD Construction

2.1.1. Paired RMS Inputs

Let $\mathcal{H} \subset \mathbb{N}_{>0}$, with $1 \in \mathcal{H}$, be the finite set of integer harmonic orders declared by the measurement or reporting procedure, and let $\mathcal{H}' = \mathcal{H} \setminus \{1\}$. For each $h \in \mathcal{H}$, $V_h \geq 0$ and $I_h \geq 0$ are the per-order RMS voltage and current magnitudes obtained over the same observation interval or, for controlled periodic steady-state tests, under the same matched operating condition. The pair is a record-specific observation because harmonic current spectra depend on terminal-voltage distortion and network conditions [21,30]. The nonfundamental RMS sums are $V_{H'}^2 \triangleq \sum_{h\in\mathcal{H}'} V_h^2$ and $I_{H'}^2 \triangleq \sum_{h\in\mathcal{H}'} I_h^2$.

2.1.2. Spectral-Product Matrix and CDD

Arranging the magnitudes as column vectors $\mathbf{V} = [V_h]_{h\in\mathcal{H}}$ and $\mathbf{I} = [I_h]_{h\in\mathcal{H}}$, the spectral-product matrix is

$$\mathbf{M} \triangleq \mathbf{V}\mathbf{I}^{\mathsf{T}}, \qquad M_{mn} = V_m I_n, \tag{1}$$

where $(\cdot)^{\mathsf{T}}$ denotes the transpose. Diagonal entries combine voltage and current of the same order; off-diagonal entries combine different orders. Each entry is an ordered product of RMS magnitudes; it is not an identified component of instantaneous power, and M_{mn} does not indicate that order m generates order n. With $\mathbf{M}_{\text{off}}$ obtained by zeroing the diagonal and $\|\cdot\|_{\text{F}}$ denoting the Frobenius norm,

$$\text{CDD}^2 \triangleq \|\mathbf{M}_{\text{off}}\|_{\text{F}}^2 = \sum_{\substack{m,n\in\mathcal{H}\\ m\neq n}} (V_m I_n)^2. \tag{2}$$

The Frobenius norm is a design choice: it is consistent with quadratic RMS aggregation, invariant to reordering of $\mathcal{H}$, and additive over disjoint entry sets. It is the square root of the sum of the squared matrix entries, so it combines the products of different harmonic orders into a single RMS-type scalar. Expanding $\|\mathbf{M}\|_{\text{F}}^2 = V_{\mathcal{H}}^2 I_{\mathcal{H}}^2$ and removing the diagonal gives the closed form

$$\text{CDD}^2 = V_{\mathcal{H}}^2 I_{\mathcal{H}}^2 - \sum_{h\in\mathcal{H}} (V_h I_h)^2, \tag{3}$$

where $V_{\mathcal{H}}^2 = V_1^2 + V_{H'}^2$ and $I_{\mathcal{H}}^2 = I_1^2 + I_{H'}^2$; evaluation requires $\mathcal{O}(|\mathcal{H}|)$ operations (Algorithm A1, Appendix A). CDD is a magnitude-only descriptor: it summarizes how the products $V_m I_n$ ($m \neq n$) are organized across harmonic orders. Its unit, V·A, is that of a product of magnitudes, and the main reading used here is the dimensionless ratio CDD/S_1 introduced below. Equation (3) is a partition of squared matrix entries rather than a power balance. *Distortion* in the name refers to nonfundamental spectral content. Section 3.1.2 illustrates the construction with a matched-THD pair before it is applied to simulated and measured records.

2.1.3. Fundamental-Related and Harmonic–Harmonic Partitions

The off-diagonal entries split into those involving the fundamental and those involving only nonfundamental orders, the latter forming the harmonic–harmonic (HH) part:

$$\text{CDD}_{1H}^2 \triangleq \sum_{n\in\mathcal{H}'} (V_1 I_n)^2 + \sum_{m\in\mathcal{H}'} (V_m I_1)^2 = V_1^2 I_{H'}^2 + I_1^2 V_{H'}^2, \tag{4}$$

$$\text{CDD}_{HH}^2 \triangleq \sum_{\substack{m,n\in\mathcal{H}'\\ m\neq n}} (V_m I_n)^2 = V_{H'}^2 I_{H'}^2 - \sum_{h\in\mathcal{H}'} (V_h I_h)^2, \tag{5}$$

with $\mathrm{CDD}^2 = \mathrm{CDD}_{1H}^2 + \mathrm{CDD}_{HH}^2$ by disjoint support. For $\mathrm{CDD} > 0$, the harmonic–harmonic fraction is

$$\eta_{HH} \triangleq \frac{\mathrm{CDD}_{HH}^2}{\mathrm{CDD}^2} \in [0,1]. \tag{6}$$

2.1.4. Magnitude-Only Scope

The definition uses magnitudes only, so, for a fixed pair of RMS-magnitude spectra, CDD is invariant to the assignment of harmonic phases. With complex RMS phasors $\underline{V}_h$ and $\underline{I}_h$ and with $(\cdot)^{\mathsf{H}}$ denoting the conjugate transpose, $|\underline{V}_m \underline{I}_n^*| = V_m I_n$, so that $\mathrm{CDD}^2 = \left\| \mathrm{offdiag}(\underline{\mathbf{V}}\,\underline{\mathbf{I}}^{\mathsf{H}}) \right\|_{\mathrm{F}}^2$: CDD retains a magnitude-only characterization of the off-diagonal structure of the complex voltage–current spectral outer product. It is therefore invariant to the individual spectral phases and to the choice of time origin, although a shift of the time origin changes the phases of the off-diagonal entries themselves. The consequences of this assumption, and the measurement and reporting requirements, are collected in Section 4.

2.2. THD-Determined and Order-Dependent Parts of CDD

Once CDD is defined, the two THD values serve as an interpretive tool. With the fundamental product $S_1 \triangleq V_1 I_1$ and the distortion indices over the declared spectral set, normalized by the fundamental [31],

$$a \triangleq \mathrm{THD}_{V,\mathcal{H}} = \frac{V_{H'}}{V_1}, \qquad b \triangleq \mathrm{THD}_{I,\mathcal{H}} = \frac{I_{H'}}{I_1}, \tag{7}$$

the question of Section 1 becomes precise: which part of CDD is fixed by (S_1, a, b), and which is not? Numerically, S_1 coincides with the single-phase fundamental apparent power $S_1 = V_1 I_1$ of IEEE Std 1459-2025 [9]; here it enters only as the common scale introduced by the fundamental normalization of a and b.

2.2.1. The THD-Determined Part

Proposition 1 (THD-determined part)**.** *For $V_1, I_1 > 0$,*

$$\mathrm{CDD}_{1H} = S_1 \sqrt{a^2 + b^2}. \tag{8}$$

Proof. Divide (4) by S_1^2: $\mathrm{CDD}_{1H}^2 / S_1^2 = I_{H'}^2 / I_1^2 + V_{H'}^2 / V_1^2 = b^2 + a^2$. □

Proposition 2 (Structure beyond THD)**.** *For $a, b > 0$ and a declared set with at least two nonfundamental orders, CDD_{HH}, and hence η_{HH}, is not a function of (S_1, a, b). Moreover, the complete set of same-order products $\{V_h I_h\}$ does not determine the off-diagonal entries.*

Proof. For the first claim, Section 3.1.2 gives two spectra with identical (S_1, a, b) and different CDD_{HH}. For the second, the rescaling $\widetilde{V}_h = c_h V_h$, $\widetilde{I}_h = I_h / c_h$, $c_h > 0$, preserves every $V_h I_h$ while mapping $V_m I_n \mapsto (c_m / c_n) V_m I_n$ for $m \neq n$. □

2.2.2. The Harmonic-Order Factor and the Factorization

Proposition 3 (Factorization of the global scalars)**.** *For $a, b > 0$, with the nonfundamental shares $p_h^H \triangleq V_h^2 / V_{H'}^2$ and $q_h^H \triangleq I_h^2 / I_{H'}^2$, $h \in \mathcal{H}'$, factoring $V_{H'}^2 I_{H'}^2$ out of (5) gives*

$$\mathrm{CDD}_{HH}^2 = V_{H'}^2 I_{H'}^2 \, \kappa, \qquad \kappa \triangleq 1 - \sum_{h \in \mathcal{H}'} p_h^H q_h^H \in [0,1]. \tag{9}$$

Hence $\mathrm{CDD}_{HH}^2 = S_1^2 a^2 b^2 \kappa$ *so that*

$$\mathrm{CDD}^2 = S_1^2\left(a^2 + b^2 + a^2 b^2 \kappa\right), \tag{10}$$

$$\eta_{HH} = \frac{a^2 b^2 \kappa}{a^2 + b^2 + a^2 b^2 \kappa}. \tag{11}$$

Moreover, κ is invariant to independent positive scaling of the nonfundamental voltage and current spectra and, when $\mathcal{H}'$ contains at least two orders, is not determined by the THD magnitudes a and b; $\kappa = 0$ if and only if the nonfundamental voltage and current are concentrated at the same single order, and $\kappa = 1$ if and only if the sets of nonfundamental orders carrying nonzero voltage and nonzero current are disjoint (disjoint supports). If $a = 0$ or $b = 0$, the harmonic–harmonic term vanishes, so $\mathrm{CDD}_{HH} = 0$ and, whenever $\mathrm{CDD} > 0$, $\eta_{HH} = 0$; in that boundary case, κ is undefined and not required; if $a = b = 0$, then $\mathrm{CDD} = 0$ and η_{HH} is not defined.

Proof. Equation (9) follows from (5) because $\sum_{h\in\mathcal{H}'}(V_h I_h)^2/(V_{H'}^2 I_{H'}^2) = \sum_{h\in\mathcal{H}'} p_h^H q_h^H$; since $V_{H'} = aV_1$ and $I_{H'} = bI_1$, it gives $\mathrm{CDD}_{HH}^2 = S_1^2 a^2 b^2 \kappa$ and, by Proposition 1, $\mathrm{CDD}_{1H}^2 = S_1^2(a^2 + b^2)$, which gives (10) and (11). For fixed a and b and at least two nonfundamental orders, the nonfundamental norms are fixed while the normalized distributions p^H and q^H can vary; therefore, κ is not determined by the THD magnitudes alone. For nonnegative shares summing to one, $\sum p_h^H q_h^H \le \sum p_h^H = 1$, with equality if and only if $q_h^H = 1$ wherever $p_h^H > 0$, that is, if and only if both are the same unit vector; and $\sum p_h^H q_h^H = 0$ if and only if no order carries both nonfundamental voltage and current, that is, if and only if the supports are disjoint.□

The factorization (10) is the central result of this section:

$$\mathrm{CDD}^2 = S_1^2\Big[\underbrace{a^2 + b^2}_{\text{fixed by THD}} + \underbrace{a^2 b^2 \kappa}_{\text{not fixed by THD}}\Big]. \tag{12}$$

Equation (10) separates the dimensional scale from the dimensionless spectral factors: S_1 sets the common VA scale of CDD, whereas a, b, and κ determine CDD/S_1. Because $V_{H'}^2 I_{H'}^2$ is the squared Frobenius norm of the nonfundamental block of $\mathbf{M}$, κ is the fraction of that block lying off its diagonal, i.e., the complement of the same-order overlap between the normalized nonfundamental squared spectra. The factor κ therefore summarizes two properties of the paired spectra: their same-order alignment and the concentration of each spectrum across harmonic orders.

As a scalar summary, κ takes the same value for many different spectral pairs, and proportional nonfundamental spectra spread over two or more orders give $\kappa > 0$: for $p^H = q^H$, $\kappa = 1 - \sum_{h\in\mathcal{H}'}(p_h^H)^2$ is the Gini–Simpson diversity index, i.e., the complement of Simpson's concentration index [32], and identical shares spread equally over N orders give $\kappa = 1 - 1/N$. Thus, κ increases both when the dominant voltage and current orders differ and when the content is spread over more orders, rather than measuring spectral disagreement alone. The two effects separate exactly: $1 - \kappa = c_{pq}\sqrt{\lambda_p \lambda_q}$, where $c_{pq} = \sum_h p_h^H q_h^H / (\sum_h (p_h^H)^2 \sum_h (q_h^H)^2)^{1/2}$ is the cosine similarity between the two share vectors and measures their same-order alignment, and $\lambda_p = \sum_h (p_h^H)^2$ and $\lambda_q = \sum_h (q_h^H)^2$ are the Simpson concentrations of the two spectra; this interpretive decomposition shows how κ responds to both alignment and concentration.

CDD is the descriptor; CDD_{1H} and CDD_{HH} are its exact disjoint parts. By Proposition 2, (S_1, a, b) are insufficient to determine CDD_{HH}; once they are specified, the remaining dependence of the global CDD quantities on order-resolved organization is captured by the single factor κ so that (S_1, a, b, κ) determine CDD, CDD_{HH}, and η_{HH} exactly. The fraction

η_{HH} is a derived evaluation quantity, fixed by (a, b, κ) through (11). Figure 1 summarizes the resulting structure of $\mathbf{M}$.

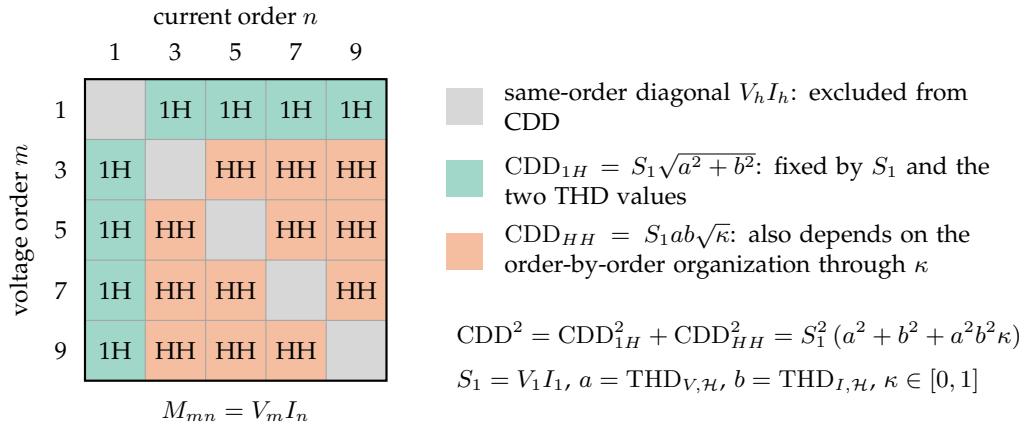


Figure 1. Spectral-product matrix over an illustrative set $\mathcal{H} = \{1, 3, 5, 7, 9\}$. Same-order entries are excluded from CDD; the Frobenius norm of the fundamental-related region is fully determined by the fundamental product and the two THD values over the declared set, whereas the harmonic–harmonic region additionally depends on the normalized harmonic-order factor κ of (9).

2.2.3. THD Bounds

Proposition 4 (THD bounds). *For $V_1, I_1 > 0$, with $a^2 + b^2 > 0$ for the bounds on η_{HH} and the last inequality strict when $a, b > 0$:*

$$\sqrt{a^2+b^2} \;\le\; \frac{\mathrm{CDD}}{S_1} \;\le\; \sqrt{a^2+b^2+a^2b^2}, \tag{13}$$

$$\begin{aligned} \eta_{HH} &\le \frac{a^2b^2}{a^2+b^2+a^2b^2} \\ &\le \min\left(\frac{a^2}{1+a^2}, \frac{b^2}{1+b^2}\right). \end{aligned} \tag{14}$$

Proof. Equation (13) is (10) with $\kappa \in [0,1]$. For (14), the right side of (11) is increasing in κ, and $\kappa \le 1$ gives the first bound; cross-multiplication shows $a^2b^2(1+a^2) \le a^2(a^2 + b^2 + a^2b^2)$, with equality only if $a = 0$, and symmetrically in b; the minimum is therefore attained only if $a = 0$ or $b = 0$. □

Corollary 1 (Necessary condition for harmonic–harmonic dominance). *$\eta_{HH} > 1/2$ requires $a^{-2} + b^{-2} < 1$; for $a = b$, this means $a > \sqrt{2}$, i.e., THD above* 141%.

THD therefore fixes CDD_{1H} exactly and sets the THD-imposed upper bound in (14), attained when $\kappa = 1$, i.e., when the nonfundamental supports are disjoint, which for $a, b > 0$ requires at least two nonfundamental orders; κ determines where, below that ceiling, a record lies. More precisely, for $a, b > 0$, the position of a record below its ceiling follows from (11):

$$\begin{aligned} \frac{\eta_{HH}}{a^2b^2/(a^2+b^2+a^2b^2)} &= \kappa\,\frac{a^2+b^2+a^2b^2}{a^2+b^2+a^2b^2\kappa}, \\ 0 \le \frac{\eta_{HH}}{a^2b^2/(a^2+b^2+a^2b^2)} - \kappa &\le \frac{\min(a,b)^2}{4}, \end{aligned} \tag{15}$$

because the difference equals $\kappa(1-\kappa)a^2b^2/(a^2+b^2+a^2b^2\kappa) \le a^2b^2/[4(a^2+b^2)]$. Up to $\min(a,b)^2/4$, which is below 0.01 whenever either THD value is below 20%, κ is therefore the position of the record between the THD-determined floor and ceiling of η_{HH}. The last inequality in (14) shows that low voltage THD alone keeps η_{HH} small irrespective of how

distorted the current is: for $a = 5\%$, $\eta_{HH} < 0.25\%$, and at the 8% voltage-THD limit that IEEE Std 519-2022 specifies at the point of common coupling for bus voltages at or below 1 kV [1], $\eta_{HH} < 0.64\%$. Corollary 1 provides a complementary screen: harmonic–harmonic dominance requires both THD values to exceed 100%, and for equal voltage and current THD the threshold is $\sqrt{2} \approx 141\%$.

2.2.4. Distinction from Spectral Nonproportionality

A natural reading of CDD, or of κ, is that it measures how differently shaped the voltage and current spectra are. The Lagrange identity gives

$$\mathrm{CDD}^2 = \underbrace{\sum_{m<n} (V_m I_n - V_n I_m)^2}_{L^2} + 2 \sum_{m<n} (V_m I_m)(V_n I_n), \tag{16}$$

with sums over $m, n \in \mathcal{H}$. Terms of the same form as the first appear in Emanuel's expansion of the complementary power $\sqrt{S^2 - P^2}$, with S and P the apparent and active power, over common orders [33]. The first term, the magnitude-spectrum nonproportionality term, satisfies $L = 0$ for nonzero $\mathbf{V}$ and $\mathbf{I}$ if and only if $\mathbf{I} = c\mathbf{V}$ for some $c > 0$, whereas the second, the same-order magnitude co-support term, remains positive whenever at least two orders each carry nonzero voltage and current. Hence, $L = 0$ does not imply $\mathrm{CDD} = 0$. In particular, an ideal frequency-independent resistive load has proportional voltage and current magnitude spectra but nonzero CDD whenever more than one order is present. Equation (16) therefore provides a structural clarification: CDD measures off-diagonal RMS-product mass, not distance or nonproportionality between the spectra. Neither term is interpreted here as a physical cross-frequency interaction.

3. Results

3.1. Interpretation and Tutorial Examples

3.1.1. Reading Guide

Table 1 lists the question each quantity answers and what determines it. The order of the rows is a reading guide for a single record, not an engineering decision procedure. Because η_{HH} depends on a and b, it compresses differences in κ when either THD is small; κ and CDD_{HH} are therefore read alongside η_{HH}. Near the measurement noise floor, κ should be interpreted cautiously; the corresponding measurement considerations are given in Section 4.1. Figure 2 shows what can be obtained from each type of archived record. When only the fundamentals and the two THD values are available, CDD_{1H} follows exactly and CDD and η_{HH} are bounded a priori; κ, CDD_{HH}, and the exact CDD require the paired per-order magnitudes.

Table 1. Reading guide for the CDD quantities of one record.

Quantity	Question Answered	Determined by
S_1	Fundamental VA scale	V_1, I_1
a, b	Aggregate voltage and current distortion	Each spectrum
CDD_{1H}	Off-diagonal mass fixed by THD	S_1, a, b
Bound (14)	Largest harmonic–harmonic share THD permits	a, b
κ	Position below that ceiling (normalized HH organization)	Shares p_h^H, q_h^H
CDD_{HH}	Absolute harmonic–harmonic magnitude	S_1, a, b, κ
η_{HH}	Relative harmonic–harmonic share	a, b, κ

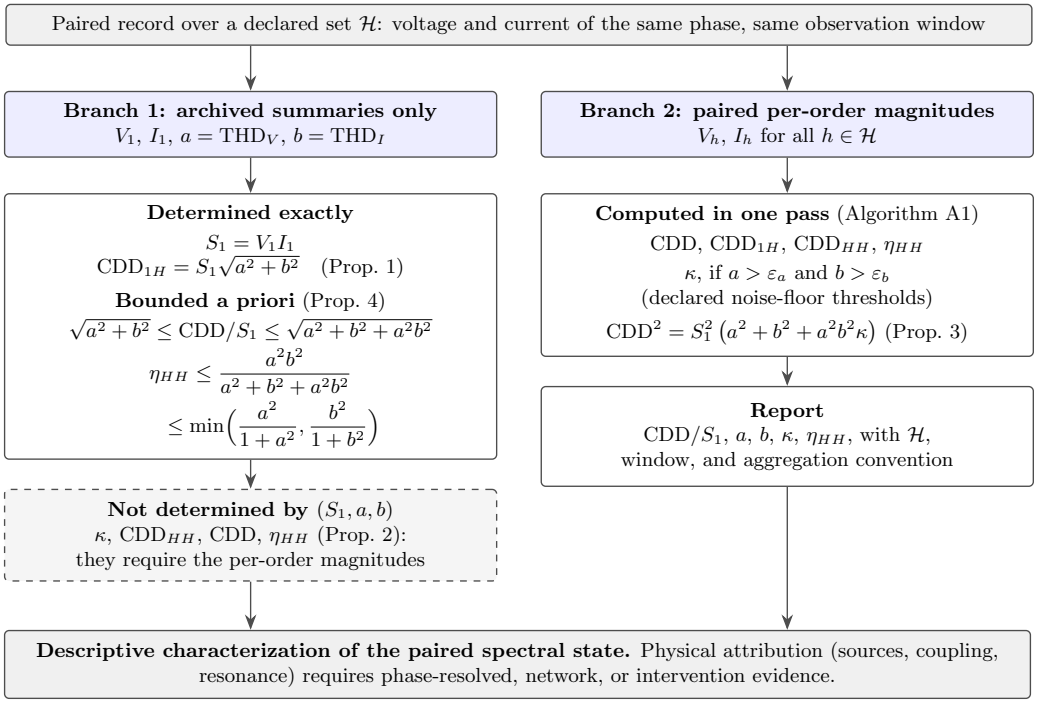


Figure 2. Quantities available from the two types of archived record. Branch 1 uses only the fundamentals and the two THD values over the declared set; Branch 2 uses the paired per-order magnitudes and Algorithm A1. The factorization applies for nonzero nonfundamental voltage and current RMS content; reporting of κ is subject to the declared measurement limits. Both branches lead to a descriptive characterization of the paired spectral state; physical attribution requires phase-resolved, network, or intervention evidence. Shading only groups the boxes (grey: common input and outcome; blue: branch headers); the dashed box lists the quantities not determined by Branch 1.

3.1.2. Constructed Matched-THD Pair

The first example isolates what THD cannot distinguish. Take $\mathcal{H} = \{1,5,7\}$, $V_1 = I_1 = 1$ per unit (p.u.), and $a = b = 10\%$. In the coincident case, $V_5 = I_5 = 0.1$ and $V_7 = I_7 = 0$. In the disjoint case, $V_5 = I_7 = 0.1$ and $V_7 = I_5 = 0$. Table 2 shows that the two cases, identical in (S_1, a, b), sit at opposite ends of the admissible range of Proposition 4: the coincident case has $\kappa = 0$ and $\eta_{HH} = 0$, whereas the disjoint case has $\kappa = 1$ and reaches the THD-imposed upper bound on η_{HH}.

Table 2. Matched-THD pair over $\mathcal{H} = \{1,5,7\}$ (p.u.).

Quantity	Coincident	Disjoint
$\mathrm{THD}_{V,\mathcal{H}}$, $\mathrm{THD}_{I,\mathcal{H}}$	10.00%, 10.00%	10.00%, 10.00%
CDD_{1H}	0.14142	0.14142
CDD_{HH}	0	0.01000
CDD	0.14142	0.14177
κ	0	1
η_{HH} (ceiling 0.4975%)	0	0.4975%

3.1.3. Matched-Voltage-THD Rectifier Example

The pair of Section 3.1.2 is constructed; an analogous situation arises in a simple nonlinear load. A single-phase diode bridge with a 1000 µF DC-link capacitor and a 60 Ω load is supplied through 0.5 Ω and 1 mH by a 120 V, 60 Hz source carrying harmonics of orders 3, 5, 7, and 11 at zero phase (all sources are sine functions that start together at $t = 0$), scaled so that $\mathrm{THD}_V = 5\%$ in every case. The supply spectra form a population of 2500 cases

generated for this study: the voltage shares (p_3, p_5, p_7, p_{11}) of the four supply harmonics are drawn from a Dirichlet$(1,1,1,1)$ distribution, i.e., uniformly over all share combinations, with a fixed random seed. This sampling distribution is a declared choice; the population is not a reconstruction of the earlier hand-screening documented in Supplementary File S1. Each case is simulated with the ngspice circuit solver (ngspice-42) and post-processed in Python 3 with NumPy (netlists and scripts in File S2) over $\mathcal{H} = \{1,3,5,\ldots,25\}$; the reported quantities are evaluated over the last 10 of 35 simulated cycles, and extending the simulation to 50 cycles changes the current THD, κ, the mean DC voltage, and the ripple by less than 10^{-6} in relative terms in ten randomly chosen cases. The voltage spectrum is taken at the ideal source, upstream of R_s and L_s, so the matched THD_V is a controlled input of the comparison, whereas the voltage THD at the rectifier terminals follows from the circuit response. Conduction is counted where the line current exceeds 0.02 A, an operational definition. The simulation starts from the ngspice operating point, with no explicit initial condition on the DC-link capacitor. All 2500 simulations completed. Figure 3 shows the circuit and the recorded quantities.

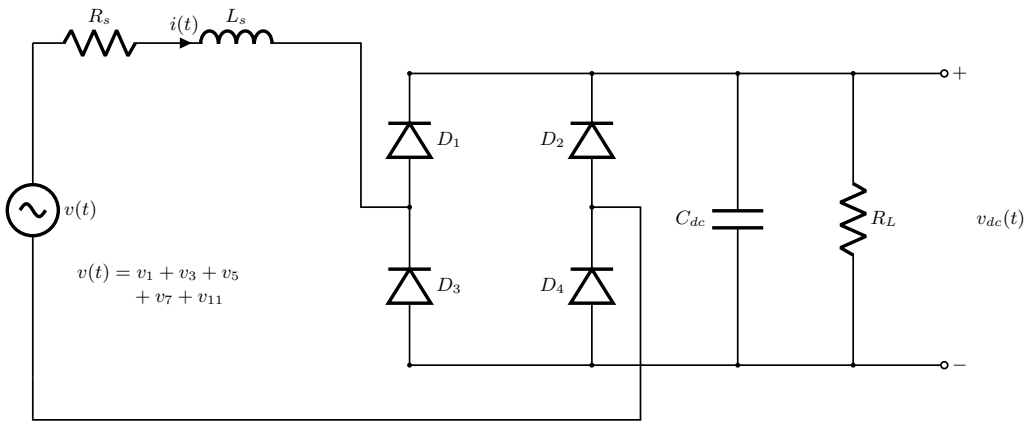


Figure 3. Simulated single-phase diode-bridge rectifier. The supply is an ideal AC source whose voltage $v(t) = v_1 + v_3 + v_5 + v_7 + v_{11}$ is the sum of the fundamental v_1 (120 V, 60 Hz) and harmonic components of orders 3, 5, 7, and 11 (series-connected sources in the netlists); $R_s = 0.5\ \Omega$, $L_s = 1$ mH, $C_{dc} = 1000\ \mu$F, $R_L = 60\ \Omega$; diode model with saturation current 1 nA, emission coefficient 1.5, series resistance 0.01 Ω, and junction capacitance 1 nF. The spectra of the supply voltage $v(t)$, taken at the ideal source upstream of R_s, and line current $i(t)$ give the CDD quantities; the DC-link voltage $v_{dc}(t)$ gives the mean DC voltage and ripple. High-value auxiliary resistors used for numerical reference (100 kΩ) are omitted. The netlists are in the Supplementary Material.

A pair of cases is eligible when the relative difference of their current THD values is below 0.5%; 161,454 of the 3,123,750 possible pairs (5.2%) meet this criterion. Among them, $|\Delta\kappa|$ has a median of 0.111, a 90th percentile of 0.293, and a maximum of 0.615, and 436 pairs (0.27%) have $|\Delta\kappa| \geq 0.5$ (Figure 4). The pair of Table 3 is the eligible pair with the largest $|\Delta\kappa|$ (population cases 1835 and 558); no rectifier-response quantity enters the selection. The example therefore shows that the contrast exists in the simulated population and is reproducible from the declared selection procedure; its frequency under practical operating conditions is not assessed. The pair counts describe this sampled population only: each spectrum enters many pairs, so the pairs are not independent observations, and no inferential statistics are computed from them.

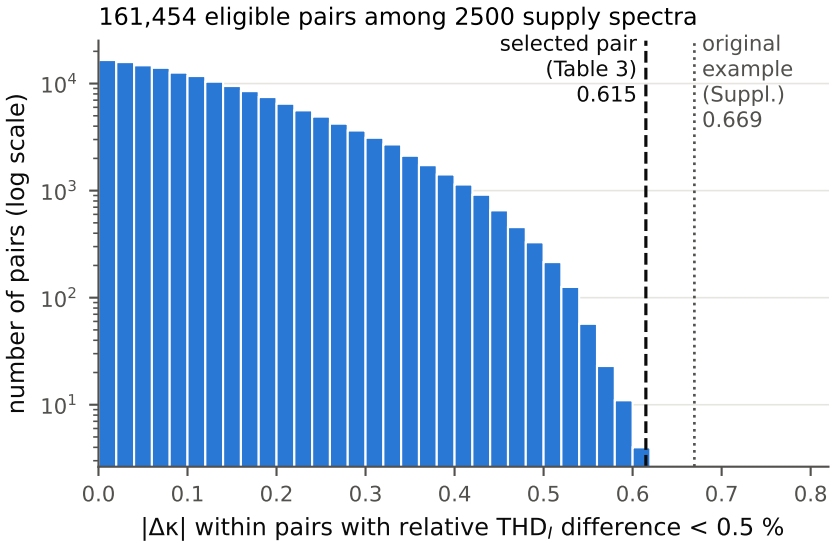


Figure 4. Distribution of $|\Delta\kappa|$ over the 161,454 eligible pairs (relative current-THD difference below 0.5%) of the 2500 simulated supply spectra; logarithmic vertical axis. The dashed line marks the selected pair of Table 3, which is the population maximum. The dotted line marks an earlier hand-screened example, which lies outside the sampled population (Supplementary Material).

Table 3. Matched-voltage-THD rectifier example (ngspice; $THD_V = 5.00\%$ in all cases): the eligible pair with the largest $|\Delta\kappa|$ in the simulated population.

Quantity	Case A	Case B	Case B, Third-Harmonic Phase 180°
Population case	1835	558	558
Dominant voltage order	11	3	3
THD_I	92.31%	92.49%	106.95%
κ	0.958	0.343	0.434
Conduction interval	61.3°	64.9°	56.8°
DC-link ripple (peak-to-peak)	14.96 V	14.27 V	16.25 V
Mean DC voltage	156.6 V	151.5 V	163.0 V

Cases A and B have equal voltage THD and nearly identical current THD, with a relative difference of 0.20%, yet κ differs by 0.615. The voltage distortion of Case A lies mainly at orders 11 and 7 ($p_{11}^H = 0.60$, $p_7^H = 0.38$) and that of Case B at order 3 ($p_3^H = 0.92$); in both, the rectifier draws most of its harmonic current at order 3 ($q_3^H = 0.70$ and 0.72). Figure 5 shows this contrast through the normalized nonfundamental voltage and current shares: Case A places its dominant voltage and current content at different orders and therefore has little same-order overlap, whereas Case B concentrates both mainly at the third harmonic. For Case B, $1 - \kappa = \sum_{h \in \mathcal{H}'} p_h^H q_h^H$ is dominated by the third-order term so that $\kappa \approx 1 - p_3^H q_3^H \approx 0.34$. The two THD values do not register this difference in order-resolved organization. The operating states also differ: at zero phase, the third harmonic flattens the voltage peak (Figure 6), so the capacitor recharges earlier, the conduction interval widens by 3.6°, and the DC-link ripple and mean DC voltage fall by 0.70 and 5.1 V, consistent with the known effect of waveform flattening on capacitor-filtered rectifiers [34,35]; the dependence of rectifier current harmonics on both the magnitude and the phase of supply-voltage harmonics is documented experimentally [8]. For conduction thresholds from 0.005 to 0.1 A, the conduction interval of Case B exceeds that of Case A by 3.2–3.7°, and the ordering of the three cases is unchanged. Under separate ±20% changes of the source inductance, capacitance, and load resistance, the relative current-THD difference did not exceed 1.10%, the separation in κ remained above 0.59, and Case B kept a 2.9–4.4° wider conduction interval, a 0.54–0.94 V lower DC-link ripple, and a 5.0–5.2 V lower mean DC voltage. In this

pair, the voltage share p_3^H alone would also separate the cases; κ adds whether the voltage distortion falls on the orders where the measured current is concentrated, which requires both spectra.

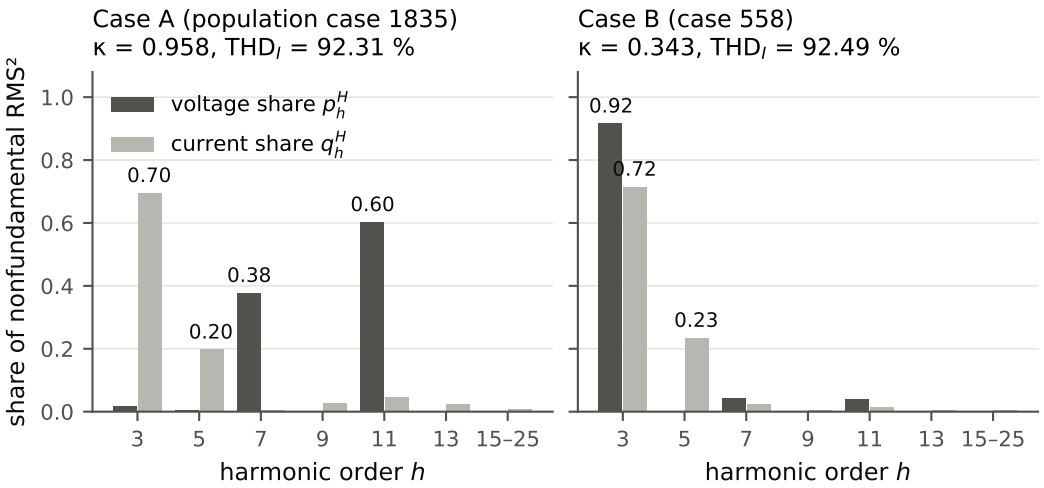


Figure 5. Normalized nonfundamental voltage and current shares of the matched-voltage-THD rectifier Cases A and B of Table 3, with the odd orders 15–25 combined into the final displayed category. In Case A, voltage distortion is concentrated mainly at the eleventh and seventh harmonics, whereas current distortion is concentrated mainly at the third harmonic, giving little same-order overlap and $\kappa = 0.958$. In Case B, both spectra are concentrated mainly at the third harmonic, which increases the same-order overlap and reduces κ to 0.343. The paired shares determine the overlap term $1 - \kappa = \sum_{h \in \mathcal{H}'} p_h^H q_h^H$; the figure describes the observed magnitude spectra.

The phase-reversed case in the third column qualifies this reading. Reversing the phase of the third harmonic leaves every voltage magnitude unchanged but makes the voltage waveform more peaked (Figure 6): the conduction interval narrows to 56.8°, below that of Case A, while κ changes only to 0.434; under the ±20% component changes, its conduction interval remains 4.0–5.0° below that of Case A. Thus, κ distinguishes how the voltage and current harmonic magnitudes are distributed and aligned across orders, whereas harmonic phase, which CDD does not retain, can materially alter how that organization appears in time-domain operation.

Across the population, the direction of this contrast is regular but not specific to κ. In all 436 eligible pairs with $|\Delta\kappa| \geq 0.5$, the member with the larger κ has the shorter conduction interval. Over all eligible pairs, the Spearman rank correlations of $|\Delta\kappa|$ with the absolute differences in mean DC voltage, ripple, and conduction interval are 0.86, 0.91, and 0.42; the voltage-only share p_3^H gives 0.94 and 0.85 for the first two, and the current concentration λ_q gives 0.75 for the conduction interval. These associations are descriptive of this population, and κ is not proposed as a predictor of rectifier operation. An earlier hand-screened example ($\kappa = 0.979$ and 0.309) came from a screening whose script was not preserved. Its $|\Delta\kappa| = 0.669$ exceeds the population maximum, and its Case B lies outside the sampled range, with $p_3^H = 0.946$ and $\kappa = 0.309$ against a population maximum of 0.927 and minimum of 0.343; it remains numerically reproducible from its netlists and is reported in the Supplementary Material.

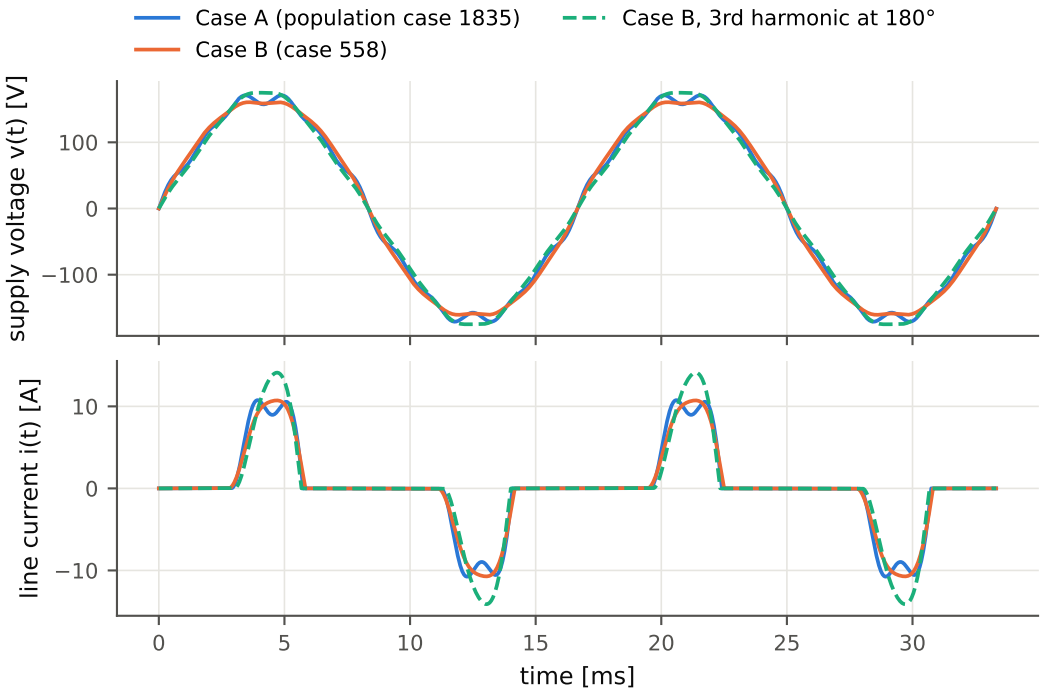


Figure 6. Supply voltage and line current over two fundamental cycles in steady state for the three cases of Table 3. With the third harmonic at zero phase, the voltage of Case B has a flattened crest; with the third harmonic at 180°, its crest is peaked and the current pulse is narrower and higher. The per-order voltage magnitudes, and hence THD_V, are identical in Case B and its phase-reversed variant.

3.1.4. Worked Measured Example

Montoya et al. report a single-phase residential record acquired over 200 ms at 15.625 kHz with an openZmeter analyzer [14]. The source tabulates magnitudes for $\mathcal{H} = \{1,3,5,7,9\}$ (Table 4); all quantities below therefore refer to this declared subset. Absolute quantities formed from nonnegative squared contributions, including CDD, CDD_{1H}, and CDD_{HH}, are lower bounds relative to an enlarged spectral set when the reported components are held fixed, whereas normalized quantities such as η_{HH} and κ are subset-dependent and need not vary monotonically. The steps follow the reading guide of Table 1.

Table 4. Published residential RMS magnitudes [14] and hand-computed quantities over $\mathcal{H} = \{1,3,5,7,9\}$.

Order h	**1**	**3**	**5**	**7**	**9**
V_h (V)	233.92	0.46	4.74	4.02	0.42
I_h (A)	2.33	0.93	0.45	0.49	0.16
$V_h I_h$ (VA)	545.03	0.43	2.13	1.97	0.07
Step 2: a, b			2.670%, 49.55%		
Step 3: CDD_{1H}			270.48 VA		
Step 4: CDD_{HH}			6.59 VA		
Step 5: CDD, η_{HH}			270.56 VA, 0.059%		
Step 6: κ, bound (14)			0.834, 0.071%		

The fundamental product is $S_1 = 233.92 \times 2.33 = 545.03$ VA. For the reported subset, $V_{H'}^2 = 39.016\ \mathrm{V}^2$ and $I_{H'}^2 = 1.3331\ \mathrm{A}^2$, giving $a = 2.670\%$ and $b = 49.55\%$. Equation (8) then gives $\mathrm{CDD}_{1H} = 270.48$ VA without using the order-by-order distribution.

The distinction appears in the HH term. From (5), $V_{H'}^2 I_{H'}^2 = 52.012\ \mathrm{V^2A^2}$ while $\sum_{h\in\mathcal{H}'}(V_h I_h)^2 = 8.617\ \mathrm{V^2A^2}$, so $\mathrm{CDD}_{HH} = 6.59$ VA. Thus, CDD = 270.56 VA, $\eta_{HH} = 0.059\%$, and $\kappa = 0.834$. The THD-imposed upper bound in (14) is 0.071%: the low voltage THD caps η_{HH}, whereas the order-resolved arrangement ($\kappa = 0.834$) places the record close to that cap. Under the illustrative sensitivity analysis of Section 4.1, κ remains within 0.820–0.848 in the widest scenario, and setting to zero the components closest to the noise floor (V_3, V_9, and I_9) changes it by at most 0.004. The quantity most sensitive to the declared voltage tolerance is η_{HH} (about $\pm 8\%$ relative) because $\eta_{HH} \approx a^2\kappa$ when $b \gg a$; its order of magnitude is unchanged.

3.2. Evaluation on Published and Measured Records

3.2.1. Protocol and Questions

The examples of Section 3.1 show how the quantities are read; the evaluation asks whether the separation between distortion level and harmonic-order organization appears in measured records. Each dataset is evaluated over a declared spectral set $\mathcal{H}$, stated in its subsection and in Table 5, and each phase of a three-phase record is treated as a single-phase record. Where record ordering is examined, ordering by decreasing η_{HH} is used consistently as the secondary ordering rule, with CDD_{HH} and, where the THD values are available, κ reported alongside; this ordering is used only to select records for further examination and is not interpreted as an engineering priority. Here, η_{HH} ranks the relative harmonic–harmonic contribution to CDD, whereas κ is reported separately as the normalized harmonic-order factor; the two are not interchangeable because a large κ can accompany a negligible harmonic–harmonic contribution when either THD value is small.

No universal numerical noise-floor thresholds ε_a and ε_b (Algorithm A1) are imposed retrospectively on these heterogeneous datasets because the source studies do not report instrument-specific per-order noise floors or uncertainties on a common basis. Accordingly, κ is computed for records with nonzero nonfundamental voltage and current content and is reported subject to the measurement limitations of Section 4.1. The pre-injection values of κ in Section 3.2.4 are not interpreted because the nonfundamental voltage content there is very small ($a \approx 0.2\%$) and the instrument-specific harmonic noise floor needed to assess the reliability of $V_{H'}$ is not reported.

The evaluation is organized around the following questions: can the distortion level change while the harmonic-order organization stays nearly fixed (Section 3.2.2); can the organization change in a way the two THD values do not determine (Section 3.2.3); how do the CDD scalars behave relative to a separately measured physical cross-order response (Section 3.2.4); when does the harmonic–harmonic part add little record differentiation beyond THD (Section 3.2.5); how does the reading depend on the declared spectral set (Section 3.2.6); and how does κ relate to simpler summaries of the same spectra (Section 3.2.7)?

Table 5 summarizes how the per-order magnitudes of each dataset were obtained, and Table 6 lists the operating parameters of each case together with its THD values, its THD-imposed ceiling on η_{HH} from (14), and the attained η_{HH} and κ. Every record lies below its ceiling, and, by (15), its position below the ceiling is given to within $\min(a, b)^2/4$ by κ.

Table 5. Datasets, declared spectral sets, and processing. Voltage and current magnitudes of a record refer to the same interval and spectral set; each phase of a three-phase record is treated as a single-phase record; no retrospective noise-floor thresholds are applied.

Dataset	Type	Records	$\mathcal{H}$	Per-Order Magnitudes
Constructed pair	Analytical	2	$\{1, 5, 7\}$	Assigned values (p.u.)
Rectifier	Simulation (ngspice-42)	2500 + phase-reversed case	odd orders 1–25	Fourier projection over the last 10 of 35 simulated cycles
Residential [14]	Published measurement	1	$\{1, 3, 5, 7, 9\}$	Tabulated by the source; 200 ms at 15.625 kHz (openZmeter)
PV inverter [19]	Published measurement	2 tests (phase *a*)	$\{3, 5, 7, 11, 13\}$	Tabulated by the source, measured and FCM-predicted; fundamentals not tabulated
Induction motor [17]	Published measurement	3 loading conditions	odd orders 1–11	Tabulated by the source (programmed supply voltage, measured current)
Wind converter [22]	Measured waveforms	16 injections, 3 phases, pre and post	1, 3, 5, 7, 11, 13, 17, 19, 23	DFT over blocks of 3 cycles, 512 samples per cycle; physical response from sequence phasors
Data center [36]	Public measurement	33,264 ($11,088 \times 3$)	$\{1, \ldots, 11\}$	10-min per-order RMS values processed according to IEC 61000-4-30 and IEC 61000-4-7 (dataset documentation); 77 days
Capacitors [37]	Public waveforms	458	$\{1, \ldots, 25\}$	Least-squares fit with a DC term and orders 1–25; normalized residual below 1% (voltage) and up to about 10% (current)

Table 6. Operating parameters, THD values, THD-imposed ceiling $a^2b^2/(a^2 + b^2 + a^2b^2)$ on η_{HH} from (14), and attained η_{HH} and κ for each case. Ranges are over records; for the data center, κ is given as the range of the three-phase medians.

Case	Parameters	a (%)	b (%)	Ceiling (%)	η_{HH} (%)	κ
Constructed, coincident/disjoint	$V_1 = I_1 = 1$ p.u.; $V_5 = I_5 = 0.1$ / $V_5 = I_7 = 0.1$	10.00	10.00	0.4975	0 / 0.4975	0 / 1
Rectifier, A/B/B at 180°	120 V, 60 Hz source with harmonics 3, 5, 7, 11; $R_s = 0.5\,\Omega$, $L_s = 1$ mH, $C_{dc} = 1000\,\mu$F, $R_L = 60\,\Omega$; population cases 1835/558/558	5.00	92.31/92.49/106.95	0.249	0.238/0.085/0.108	0.958/0.343/0.434
Residential	Single-phase record; $V_1 = 233.92$ V, $I_1 = 2.33$ A	2.67	49.55	0.071	0.059	0.834
PV inverter, Tests 7/8	10 kW, three-phase; same five stimuli at 1%/2%; grid impedance inserted	2.145/4.255 *	3.792/7.581 *	0.035/0.138	– †	0.845/0.853
Motor, no torque/half-rated/rated	Single-phase; $V_1 = 216.7/216.9/216.9$ V; supply harmonic magnitudes and angles differ among conditions	15.64/15.54/16.23	77.97/67.08/73.93	2.30/2.24/2.45	1.515/1.588/2.003	0.655/0.704/0.813
Wind converter, V_5^+ post-injection	220 V per phase, 50 Hz, rated power, LC output filter; injected harmonic nominally 4% of the fundamental	3.76–3.93	9.89–12.11	0.12–0.13	0.003–0.005	0.023–0.038
Data center	Point of connection of a university data center; 10-min records per phase	1.38–5.78	7.5–10.8	$\leq$0.250	$\leq$0.223	0.78–0.87
Capacitors	Two metallized-polypropylene capacitors; 10 excitation families at 23 supply voltages from 209 to 231 V, 60 Hz	0.31–12.50	1.3–62.2	$\leq$1.478	$\leq$1.105	0.518–0.925

* THD values published by the source. † Not computed because the fundamentals are not tabulated.

3.2.2. Level Change with Nearly Constant Normalized HH Organization

Yahyaie and Lehn applied programmed harmonic-voltage stimuli to a commercial 10 kW three-phase grid-tied photovoltaic (PV) inverter, measured voltage and current harmonics at the point of common coupling after inserting a grid impedance, and identified the frequency-coupling matrix (FCM) of the inverter from separate single-harmonic stimuli [19]. Their Tests 7 and 8 apply the same five stimuli at 1% and 2%, and the source reports phase-*a* magnitudes, measured and FCM-predicted, for $\mathcal{H}' = \{3, 5, 7, 11, 13\}$. Because the fundamentals are not tabulated, only the quantities that do not require them, CDD_{HH} and κ, are computed; both are exact for this subset. Doubling the stimuli raises the THD values published by the source from 2.145% to 4.255% (voltage) and from 3.792% to 7.581%

(current) and multiplies CDD_{HH}, computed directly from the tabulated magnitudes, by 4.01 (2.415 to 9.685 VA), while κ moves only from 0.845 to 0.853. This factor need not equal the product of the published THD ratios because that relation would additionally require an unchanged fundamental product S_1 and an identical spectral set. This near invariance is consistent with an approximately scaled order distribution in the reported FCM response at the fixed operating point; the residual change is small and is not attributed here to a specific cause. The FCM-predicted spectra reproduce CDD_{HH} to within 1.1% and κ to within 0.003 in both tests: a separately identified physical model that reproduces the measured spectra also reproduces the CDD quantities computed from those spectra. The FCM coefficient denoted $M^{7,5}_{P,N}$ in [19] and the product $V_5 I_7$ share an index pattern but not a meaning: the first is an identified input–output coefficient of the inverter, the second a product of magnitudes of one observed state.

3.2.3. Organization Change Beyond THD

Fauri published measured RMS spectra of a single-phase induction motor supplied by a distorted voltage at three mechanical loading conditions: no torque, half-rated, and rated [17]; the loading condition is set by the experiment. Only the measured columns of the source's Tables II–IV are used; the crossed-frequency admittance model of the source is not part of the calculation (Table 7).

Table 7. Induction-motor records [17]: THD, CDD quantities, and the factor κ of (9).

Condition	a (%)	b (%)	CDD_{HH} (VA)	η_{HH} (%)	κ
No torque	15.636	77.967	16.54	1.515	0.655
Half-rated	15.538	67.078	14.95	1.588	0.704
Rated	16.234	73.925	18.50	2.003	0.813

The clearest contrast is between no torque and rated load. The nonfundamental product $V_{H'} I_{H'}$, which sets the scale of CDD_{HH} in (9), changes by only 0.32%, whereas CDD_{HH} increases by 11.79%. At fixed scale, the change in κ alone would produce an 11.44% increase in CDD_{HH}; correspondingly, the same-order term $\sum_{h \in \mathcal{H}'} (V_h I_h)^2$ decreases by 45.5%. Across the three conditions, κ rises from 0.655 (no torque) to 0.704 (half-rated) and 0.813 (rated), and η_{HH} follows the same sequence, whereas a gives rated $>$ no torque $>$ half-rated and b gives no torque $>$ rated $>$ half-rated. At a nearly fixed harmonic–harmonic scale, the paired spectra therefore changed in their order-resolved organization, which the two THD values do not register.

Because the source reports neither per-order uncertainties nor its instrument class, the sensitivity of these readings was examined under the illustrative error scenarios described in Section 4.1, with 10^5 draws per scenario. The increase of CDD_{HH} from no torque to rated load remained positive in at least 99.99% of the draws whenever the errors were independent across orders or partly shared (central 95% range +5.0% to +19.1% in the widest combined scenario), and in 97.5% when each record received its own common gain on the harmonic orders, as after a recalibration between tests. The κ ordering of the three conditions was preserved in every draw. Under the same scenarios, the 0.32% change of the scale is not distinguishable from zero (−5.9% to +7.0%); the reading is that CDD_{HH} changes by more than its scale can account for. The voltage THD of the no-torque and half-rated conditions differs by only 0.098 percentage points, and that ordering was preserved in 57% of the draws, the η_{HH} ordering of the same two conditions in 89%. Under these illustrative scenarios, the orderings by κ and CDD_{HH} are therefore robust, whereas the orderings of the no-torque and half-rated conditions by a or η_{HH} are not. The source supplied each test with a constant fundamental voltage and a random harmonic content,

which differs among the three reported conditions (Tables II–IV of [17]). The observed contrast is therefore not attributed to torque; establishing a torque-specific effect would require additional phase-resolved, network, or controlled-intervention evidence. With only three reported operating conditions and no per-order measurement uncertainties available from the source, these orderings are treated as descriptive rather than inferential.

3.2.4. Physical Cross-Order Response Under Controlled Injection

This subsection tests the distinction between CDD spectral-product structure and physical cross-order response using controlled injections for which the response is established independently of CDD. The waveform records were provided with permission by W. Xu and originate from harmonic-injection experiments conducted by the research team of Y. Sun at Shandong University on a grid-connected wind-turbine converter system with an inductor–capacitor (LC) output filter, operated at rated power from a programmable supply set to 220 V per phase at 50 Hz; the related modeling study is reported in [22], and the CDD analysis presented here is independent of the original study.

In each test, a single positive- or negative-sequence voltage harmonic of order $m \in \{3, 5, 7, 11, 13, 17, 19, 23\}$, nominally 4% of the fundamental, was superimposed on the supply, and three-phase voltage and current waveforms were recorded before and after the injection, giving 16 injections. Each waveform block spans three fundamental cycles with 512 samples per cycle; per-order phase magnitudes over $\mathcal{H} = \{1, 3, 5, 7, 11, 13, 17, 19, 23\}$ are obtained by the discrete Fourier transform, and each phase is then evaluated as a separate single-phase CDD record. Record labels were checked against the sequence of the injected voltage component. For $m = 19$ and 23, two interchanged post-injection labels were reassigned. For the same orders, the positive-sequence pre-injection blocks still contain the preceding injection, so the negative-sequence pre-injection blocks were used as baselines.

Physical response is evaluated separately in the sequence domain. If a voltage stimulus $\underline{V}_m^{\sigma}$ produces a current response $\underline{I}_n^{\tau}$, with $\sigma, \tau \in \{+, -\}$, define the experimental single-stimulus response ratio

$$G^{\mathrm{exp}}_{n^{\tau}, m^{\sigma}} \triangleq \frac{|\Delta \underline{I}_n^{\tau}|}{|\Delta \underline{V}_m^{\sigma}|}, \tag{17}$$

where the pre- and post-injection sequence phasors are synchronized to the positive-sequence fundamental. This ratio is used only to quantify the measured response to the imposed stimulus; it is not identified here as a converter coupling coefficient.

Among the 16 injections, the largest measured cross-order sequence response is $V_5^+ \rightarrow I_3^-$, with $G^{\mathrm{exp}}_{3^-,5^+} = 0.0250$ S. In the resulting phase-domain states, I_3 rises to 0.21–0.24 A, and the harmonic-order product $V_5 I_3$ carries 79–90% of CDD^2_{HH} (Table 8). Thus, for this intervention, the order pair $(5, 3)$ associated with the independently established sequence-domain response is also prominent in the phase-domain spectral-product matrix. The physical response is identified by the controlled intervention and the sequence-domain phasors, which establish which sequence component responded; CDD records how that response appears in the paired magnitude spectra. The prominence of $V_5 I_3$ is, however, partly structural: the injected fifth-order component dominates the nonfundamental voltage spectrum in this test, so every measured current harmonic forms a product with a comparatively large V_5. The post-injection spectra remain strongly same-order concentrated: $V_5 I_5 = 10.6$–13.1 VA, compared with $V_5 I_3 = 1.8$–1.9 VA. Correspondingly, the post-injection values are $\kappa = 0.023$–0.038 and $\eta_{HH} < 0.005\%$, well below the THD-imposed ceilings of Table 6.

Table 8. Injection of V_5^+: phase-domain CDD quantities of the post-injection states over $\mathcal{H} = \{1, 3, 5, 7, 11, 13, 17, 19, 23\}$. The tabulated currents and products are phase-domain quantities; the physical response ratio $G^{\text{exp}}_{3^-,5^+}$ is evaluated separately from sequence phasors using (17).

Phase	I_3 Pre→Post (A)	$V_5 I_3$ (VA)	$V_5 I_5$ (VA)	Share *	κ	η_{HH} (%)
a	0.003 → 0.212	1.782	13.14	79.2%	0.023	0.0030
b	0.015 → 0.236	1.945	10.65	84.3%	0.038	0.0047
c	0.036 → 0.223	1.924	11.20	90.2%	0.032	0.0042

* Share of CDD^2_{HH} carried by the product $V_5 I_3$.

Across all 16 injections, after averaging the phase-domain products over the three independently evaluated phases, the current order of the largest sequence-domain cross-order response coincides in four of the 16 cases with the current order of the largest cross-order product $V_m I_n$ involving the injected order m. In most of the remaining cases, the largest such product is $V_m I_5$, which pairs the injected-order voltage with the fifth-order current already present in the measured state. The Spearman correlation of the largest sequence-domain response ratio is $\rho_s = 0.11$ with κ (95% confidence interval $[-0.41, 0.58]$) and $\rho_s = -0.01$ with η_{HH} ($[-0.50, 0.49]$) [38]; with 16 injections, the two-sided 5% permutation threshold is $|\rho_s| = 0.50$, so neither coefficient reaches it, and the wide intervals include zero and remain compatible with moderate associations in either direction. For example, V_5^+ gives $G^{\text{exp}}_{3^-,5^+} = 0.0250$ S with $\kappa = 0.031$, whereas V_{11}^- gives a maximum cross-order response ratio of 0.0029 S with $\kappa = 0.198$. These results show that the harmonic-order pair associated with a known physical response can be prominent in the resulting phase-domain product matrix while the global CDD scalars remain small. Accordingly, $V_m I_n$, κ, and η_{HH} should not be interpreted as physical coupling coefficients or, on the evidence here, as proxies for coupling strength.

3.2.5. Regimes with Small Harmonic–Harmonic Contribution

Long-Term Field Records

The public dataset of Garrido-Zafra et al. contains 11,088 ten-minute records over 77 days at the point of connection of an operational university data center, with per-order RMS voltage and current magnitudes for each phase through $h = 11$ [36,39]. Each phase–time pair is treated as one single-phase record over $\mathcal{H} = \{1, \ldots, 11\}$, giving 33,264 records; no sequence transformation or phase information is used, so the documented current-polarity inversion does not affect the results.

The median η_{HH} is 0.031%, 0.076%, and 0.073% for phases A, B, and C, with maxima of 0.054%, 0.223%, and 0.214%. Across all records, $\eta_{HH} \leq 0.223\%$, so CDD^2 lies almost entirely in the THD-determined fundamental-related partition, consistent with the THD-imposed ceilings of Proposition 4. The Spearman rank correlation between η_{HH} and a is 0.9966, and the ten largest values of each occur in the same ten records; for this installation, η_{HH} adds little extreme-record reordering beyond voltage THD.

Controlled Capacitor Records

The public database associated with Spavieri et al. contains waveforms of two metallized-polypropylene capacitors supplied by a programmable 60 Hz source [37,40]. For each capacitor, ten programmed excitation families (three IEC-based, five IEEE-based, one PRODIST-based, and a sinusoidal reference) are applied at 23 supply voltages from 209 to 231 V; with two voltages absent from one family, the archive holds 458 conditions. Per-order magnitudes over $\mathcal{H} = \{1, \ldots, 25\}$ are obtained by a least-squares fit that includes a DC term and orders 1–25, the DC term being excluded from the spectral quantities; the normalized fit residual is below 1% for voltage and reaches about 10% for current. Voltage THD ranges from 0.31% to 12.50%, $\eta_{HH} \leq 1.11\%$, and the Spearman coefficient between

η_{HH} and a is 0.9975; restricting the set to records with a normalized current residual below 5% (313 records) or 2% (143 records) gives 0.9983 and 0.9959. Both repeated-record datasets thus provide examples of conditions in which the harmonic–harmonic part remains a small fraction of CDD and adds little record reordering beyond voltage THD.

3.2.6. Robustness to the Declared Spectral Set

Because normalized quantities are not monotone in $\mathcal{H}$, the η_{HH} ordering was recomputed under nested truncation with common-order magnitudes held fixed. Here, $H_{\max}$ denotes the highest retained harmonic order. For the data center, the Spearman coefficient with the reference ordering ($H_{\max} = 11$) is 0.957 at $H_{\max} = 3$ and reaches 0.997 at $H_{\max} = 7$; the ten top-ranked records coincide with the reference at $H_{\max} = 7$, 9, and 10, and nine of them at $H_{\max} = 8$. For the capacitors (reference $H_{\max} = 25$), the coefficient is below 0.55 for $H_{\max} \leq 4$ and lies between 0.975 and 0.999 for $5 \leq H_{\max} \leq 24$; from $H_{\max} = 5$, the top-10% set lies within the same programmed family as in the reference, while none of the ten top-ranked records coincides with the reference for $H_{\max} \leq 18$. In these two datasets, coarse ordering thus stabilizes before fine ordering, and the declared spectral set should accompany any reported ranking.

3.2.7. What κ Summarizes Relative to Simpler Summaries

Table 9 compares κ with simpler summaries of the same normalized nonfundamental spectra: the same-order alignment c_{pq}, the joint concentration $\sqrt{\lambda_p \lambda_q}$, the Simpson concentrations λ_p and λ_q, the largest shares $\max p$ and $\max q$, and the Hellinger distance $d_{\mathrm{H}} = (1 - \sum_h \sqrt{p_h^H q_h^H})^{1/2}$. The exact identity $1 - \kappa = c_{pq}\sqrt{\lambda_p \lambda_q}$ shows that κ combines alignment and joint concentration, and their relative weight depends on the dataset. In the motor contrast, about two-thirds of the change in $\log(1 - \kappa)$ from no torque to rated load corresponds to alignment (c_{pq} falls from 0.954 to 0.639), under a logarithmic partition that is algebraic rather than causal. In the residential record, $\kappa = 0.834$ accompanies low alignment ($c_{pq} = 0.338$): the voltage and current content concentrate at different orders. Across the 458 capacitor records, in contrast, κ is close to a monotone function of the joint concentration: its Spearman rank correlation with $\sqrt{\lambda_p \lambda_q}$ is -0.98, and only 4.5% of the 104,653 record pairs are ordered differently. For these records, κ and the joint concentration produce nearly the same ranking. This is expected because the current spectrum follows from the voltage spectrum through the capacitor law ($q_h^H \propto h^2 p_h^H$): κ computed from the voltage spectrum alone has a rank correlation of 0.998 with the measured value. The other summaries order between 18% and 29% of the capacitor pairs differently from κ, and the Hellinger distance, which measures the difference between the two distributions rather than their concentration-weighted overlap, orders 47% of the pairs differently, close to the 50% expected for unrelated orderings. The comparison demonstrates descriptive differences among spectral summaries, without establishing superior predictive or diagnostic performance of κ.

Table 9. Values of κ and of simpler summaries of the same normalized nonfundamental spectra. The identity $1 - \kappa = c_{pq}\sqrt{\lambda_p \lambda_q}$ holds exactly. Capacitor records: median over the 458 refitted records; across these records, κ and $\sqrt{\lambda_p \lambda_q}$ have a Spearman correlation of -0.98 (ranges and pairwise orderings in the Supplementary Material).

Record	κ	c_{pq}	$\sqrt{\lambda_p \lambda_q}$	λ_p	λ_q	$\max p$	$\max q$	d_{H}
Residential [14]	0.834	0.338	0.490	0.503	0.477	0.576	0.649	0.602
Motor, no torque [17]	0.655	0.954	0.362	0.282	0.464	0.418	0.620	0.200
Motor, half-rated	0.704	0.918	0.322	0.283	0.368	0.422	0.522	0.225
Motor, rated	0.813	0.639	0.293	0.256	0.334	0.383	0.486	0.357
Capacitors (458), median	0.804	0.741	0.242	0.251	0.267	0.333	0.427	0.387

4. Discussion

4.1. Measurement and Reporting

In metrological terms, CDD is the result of a specified calculation applied to the per-order RMS quantities produced by a declared measurement procedure [41]. It inherits the pairing, windowing, grouping, and noise-floor treatment of the procedure that produced $\{(V_h, I_h)\}$ [2,42]; direct comparisons across records therefore require a common declared set and processing convention [43], as also observed for amplitude-only distortion indices, whose values depend on frequency resolution and grouping [44].

When paired per-order magnitudes are available from the harmonic-analysis procedure, CDD can be computed from that output without additional measurement channels; Appendix A gives a single-pass procedure. With common-order magnitudes held fixed, adding an order $h^\star$ increases CDD^2 by $V_{\mathcal{H}}^2 I_{h^\star}^2 + I_{\mathcal{H}}^2 V_{h^\star}^2 \geq 0$, with $V_{\mathcal{H}}$ and $I_{\mathcal{H}}$ evaluated before $h^\star$ is added, so CDD computed on a subset is a lower bound; normalized quantities such as η_{HH} and κ carry no such monotonicity.

Because temporal RMS aggregation and cross-order product formation do not commute in general, CDD computed from aggregated magnitudes differs from the aggregate of window-level CDD values, and the aggregation level must be declared. For quadratic aggregation over equally weighted windows, the mean of the window-level CDD^2 minus the CDD^2 of the aggregated magnitudes equals exactly $\sum_{m \neq n} \mathrm{cov}(V_m^2, I_n^2)$, with the covariances taken over the windows. IEEE Std 1459-2025 illustrates in Annex A that the observation and averaging convention can materially change an RMS result [9].

Where the spectral magnitudes come from a least-squares harmonic fit, a normalized fit residual, conceptually analogous to the residual-based goodness-of-fit of Annex E of IEEE Std 1459-2025 [9], can be checked before CDD is evaluated; it is not itself an uncertainty estimate. For a fixed declared set $\mathcal{H}$ and uncorrelated inputs with standard uncertainties $u(V_h)$, $u(I_h)$, first-order propagation of (3) gives

$$u^2(\mathrm{CDD}) \approx \frac{1}{\mathrm{CDD}^2} \sum_{h \in \mathcal{H}} \Big[V_h^2 \left(I_{\mathcal{H}}^2 - I_h^2\right)^2 u^2(V_h) + I_h^2 \left(V_{\mathcal{H}}^2 - V_h^2\right)^2 u^2(I_h) \Big]; \tag{18}$$

when measurement errors are correlated across harmonic orders or between voltage and current, the covariance terms of the full input covariance matrix must be added. As $\mathrm{CDD} \to 0$, first-order propagation may be inadequate and a Monte Carlo treatment may be preferable. This measurement uncertainty is distinct from the sensitivity to the declared set discussed above. Because κ normalizes the harmonic–harmonic term by $V_{H'}^2 I_{H'}^2$, it should not be interpreted when either nonfundamental RMS norm is comparable to the measurement noise floor or uncertainty; in that regime, the absolute CDD_{HH}, interpreted relative to its measurement uncertainty, together with the THD-imposed ceiling on η_{HH}, provides the relevant scale. The datasets of Section 3.2 do not report per-order uncertainties, so (18) is not evaluated there. Instead, the measured examples of Sections 3.1.4 and 3.2.3 are accompanied by an illustrative sensitivity analysis under declared assumptions; it is not an uncertainty budget of the original measurements. Each per-order magnitude receives a uniform error: rounding to half of the last published digit; for nonfundamental voltages, the maximum permissible error of IEC 61000-4-7 for voltage harmonics, ±5% of the reading when V_h is at least 1% of the nominal voltage and ±0.05% of the nominal voltage otherwise [2,45]; for the fundamental voltage, an assumed relative error of ±0.1% of the declared voltage; and, for currents, hypothetical relative errors of ±1, ±3, or ±5% on the harmonic orders and ±0.5% on the fundamental because no verified per-order current tolerance is available. The fundamental and the harmonic orders are perturbed

separately. Errors are independent across orders, share a common component within the nonfundamental block of each spectrum ($\rho \approx 0.5$), or are fully common within that block ($\rho = 1$); here $\rho = 1$ denotes a common gain on the harmonic orders of one spectrum, not perfect correlation between instruments or between tests. Under such a common gain, κ is invariant by construction, whereas a and b change because the fundamental error is drawn separately. The protocol, scripts, and results are included in the Supplementary Material.

4.2. Physical Interpretation

Over a common fundamental period, distinct orders are orthogonal, and cycle-average active power retains only same-order terms [46]; when phases are retained, cross-order products contribute to sum- and difference-frequency terms of the instantaneous power $p(t) = v(t)i(t)$ whose amplitudes require coherent phasor aggregation. CDD therefore characterizes the magnitude organization of the paired spectra, whereas phase-coherent reconstruction and source-oriented interpretation require phase information, network data, or a physical model. An exact algebraic identity relates CDD to the RMS apparent power of IEEE Std 1459-2025. With $S_{\mathcal{H}} = V_{\mathcal{H}} I_{\mathcal{H}}$, which equals the single-phase apparent power $S = VI$ of that standard when the waveforms carry no dc, interharmonic, or other content outside $\mathcal{H}$ [9], expanding $V_{\mathcal{H}}^2 I_{\mathcal{H}}^2$ by orders gives

$$S_{\mathcal{H}}^2 = S_1^2 + \mathrm{CDD}^2 + \sum_{h \in \mathcal{H}'} (V_h I_h)^2, \tag{19}$$

that is, Equation (3) written with the fundamental and nonfundamental same-order products separated. CDD therefore organizes part of the magnitude content of $S_{\mathcal{H}}$, and $S_{\mathcal{H}}$, S_1, and CDD determine the sum of the squared nonfundamental same-order products. Equation (19) is a relation among RMS magnitudes over the same declared set, not a power decomposition. Active power P depends on the voltage–current phase differences at the contributing orders, the fundamental reactive power Q_1 on the fundamental phase difference, and the power factor P/S combines the resulting active power with the RMS apparent power; these quantities are evaluated with the corresponding phase-resolved definitions of IEEE Std 1459-2025, alongside the magnitude organization that CDD summarizes.

The Lagrange identity links the RMS-product representation to power-theory quantities. Let $A_{\mathcal{H}} = \sum_{h \in \mathcal{H}} V_h I_h$ denote the same-order RMS-product sum, and let L be the magnitude-spectrum nonproportionality term defined in (16). It follows that

$$S_{\mathcal{H}}^2 = A_{\mathcal{H}}^2 + L^2, \tag{20}$$

that is, $A_{\mathcal{H}} \leq S_{\mathcal{H}}$, with the difference of squares fixed by L. When phases are available, the active power over the declared set is $P_{\mathcal{H}} = \sum_{h \in \mathcal{H}} V_h I_h \cos \phi_h$, with ϕ_h the voltage–current phase difference at order h, and the power factor over the declared set is $PF_{\mathcal{H}} = P_{\mathcal{H}}/S_{\mathcal{H}}$. Since $|P_{\mathcal{H}}| \leq A_{\mathcal{H}}$, Equation (20) yields

$$|PF_{\mathcal{H}}| \leq \frac{A_{\mathcal{H}}}{S_{\mathcal{H}}} = \sqrt{1 - \frac{L^2}{S_{\mathcal{H}}^2}} \tag{21}$$

and, for $Q_F = \sqrt{S_{\mathcal{H}}^2 - P_{\mathcal{H}}^2}$,

$$Q_F^2 - L^2 = A_{\mathcal{H}}^2 - P_{\mathcal{H}}^2 \geq 0. \tag{22}$$

Here Q_F is the power-triangle reactive power that IEEE Std 1459-2025 includes through Fryze's operational method and whose use it deprecates [9]; it serves only as an analytical comparison and is distinct from the fundamental reactive power Q_1. The magnitude spectra therefore fix the largest power factor attainable by any phase assignment, and

L is the smallest Q_F compatible with them; both bounds are attained when all nonzero same-order products have the same phase difference, either 0 at every order or π at every order. When the declared set covers the whole waveform content, $PF_{\mathcal{H}}$ is the power factor P/S of IEEE Std 1459-2025 [9]. With a sinusoidal voltage, $A_{\mathcal{H}} = S_1$ and the bound reduces to $1/\sqrt{1+b^2}$, the factor that multiplies the fundamental displacement factor in $PF = \cos\phi_1/\sqrt{1+b^2}$. By (16), $L \leq$ CDD; the bounds in (21) and (22) are properties of the RMS representation expressed through L, not additional diagnostic properties of CDD.

Table 10 evaluates these relations for the residential record of Section 3.1.4, whose source also tabulates the phases [14]: over $\mathcal{H} = \{1,3,5,7,9\}$, $|PF_{\mathcal{H}}| = 0.587$ lies below the bound 0.903 fixed by the magnitudes, and L lies below both Q_F and CDD. Changing only the phases leaves CDD, L, and $A_{\mathcal{H}}/S_{\mathcal{H}}$ unchanged, whereas $P_{\mathcal{H}}$, Q_1, and $PF_{\mathcal{H}}$ change and require the phase-resolved definitions. Phase-resolved decompositions such as the currents' physical components and the conservative power theory [15,16] express the power factor through the same ratio P/S, so (21) also bounds that ratio; the bound does not extend to their individual current or power components, which are not identified with the products $V_m I_n$.

Table 10. Analytical relations of Equations (20)–(22) evaluated for the residential record (Table 4) over $\mathcal{H} = \{1,3,5,7,9\}$, with the rounded magnitudes and phases published by the source [14]. The relations are algebraic and do not constitute a power decomposition.

Quantity	Value	Role
$S_{\mathcal{H}} = V_{\mathcal{H}} I_{\mathcal{H}}$	608.50 VA	Product of RMS norms; S of IEEE Std 1459-2025 when $\mathcal{H}$ covers the content
$A_{\mathcal{H}} = \sum_h V_h I_h$	549.63 VA	Same-order RMS-product sum
L	261.11 VA	Magnitude-spectrum nonproportionality term, (16); $S_{\mathcal{H}}^2 = A_{\mathcal{H}}^2 + L^2$
CDD	270.56 VA	Magnitude-only descriptor; $L \leq$ CDD
$P_{\mathcal{H}}$	357.14 W	Requires phases
$\lvert PF_{\mathcal{H}}\rvert$	0.587	Requires phases
$A_{\mathcal{H}}/S_{\mathcal{H}}$	0.903	Largest $\lvert PF_{\mathcal{H}}\rvert$ for these magnitudes, (21)
Q_F	492.67 VA	Requires phases; $Q_F \geq L$, (22)

The present definition covers single-phase, periodic steady-state records with integer harmonic orders; sequence-resolved three-phase inputs and interharmonic bins require a separately declared indexing. A three-phase formulation, in which harmonic order and symmetrical-component sequence index a composite spectral-product matrix and same-order cross-sequence products form a separate region, is left to a separate study.

4.3. Evidence and Scope

By Propositions 1–4, (S_1, a, b) determine CDD_{1H} and bound CDD and η_{HH}, whereas κ locates a record between those bounds and, by (15), is its position below the THD ceiling to within $\min(a,b)^2/4$. The evaluated records show both kinds of change. In the PV-inverter tests, both THD values approximately double at nearly constant κ; in the motor records, the harmonic–harmonic scale remains nearly unchanged under the illustrative error scenarios while CDD_{HH} increases by about 12% through κ; and in the rectifier population, equal voltage THD and current THD within 0.5% coexist with differences in κ of up to 0.615.

What κ adds to simpler order-resolved summaries depends on the dataset. In the motor contrast, about two-thirds of its change is a change of same-order alignment, which no single-spectrum summary carries. Across the capacitor records, in contrast, κ is nearly a monotone function of the joint concentration (Spearman -0.98) because the current spectrum follows from the voltage spectrum through the capacitor law. In the rectifier population, the voltage-only share p_3^H is associated with the difference in mean DC voltage at least as strongly as κ, and the current concentration λ_q is more strongly associated with the difference in conduction interval. These comparisons establish a descriptive role for κ, the quantity that enters the exact factorization of CDD; they do not show a consistent

advantage over simpler order-resolved summaries, so its incremental value is assessed case by case.

Two boundaries frame these readings. First, CDD is magnitude-only. Reversing the phase of the third supply harmonic of rectifier Case B changes its conduction interval by 8.2°, more than the 3.6° separating Cases A and B, while κ changes by 0.09; and in the controlled injections, the order pair associated with a physically established response is prominent in the product matrix while the global CDD scalars remain small. Physical response and attribution are therefore supplied by phase-resolved, network, or intervention evidence [47], with CDD characterizing the accompanying change in the paired magnitude spectra. Second, Proposition 4 keeps η_{HH} small whenever voltage THD is small regardless of the current THD: in the data-center and capacitor records, CDD^2 lies almost entirely in its THD-determined part. This identifies when the harmonic–harmonic part adds little to a scalar reading; it does not change what κ describes. Because, in the two repeated-record datasets, coarse orderings stabilize before fine ones under truncation of $\mathcal{H}$, the declared set, the observation window, and the aggregation convention accompany any reported value or ranking.

Controlled hardware experiments on power electronic converters, with before-and-after changes in supply distortion or filter configuration, could test the incremental engineering utility of κ relative to simpler order-resolved summaries.

5. Conclusions

Total harmonic distortion summarizes the voltage and current spectra separately; the Cross-Order Distortion Descriptor characterizes the off-diagonal organization of their paired RMS magnitudes across harmonic orders. Its exact factorization, $\mathrm{CDD}^2 = S_1^2(a^2 + b^2 + a^2b^2\kappa)$, separates a fundamental-related part determined by the fundamental product and the two THD values from a harmonic–harmonic part that additionally depends on the normalized factor κ, and κ is, to within $\min(a, b)^2/4$, the position of a record below the THD-imposed ceiling on the harmonic–harmonic fraction.

The simulated rectifier population and the reported motor and photovoltaic-inverter spectra illustrate this separation. A rectifier pair selected from a documented population of 2500 simulated supply spectra has equal voltage THD, nearly equal current THD, and $\kappa = 0.96$ and 0.34; measured motor records change their harmonic–harmonic organization at a nearly unchanged scale under illustrative error scenarios; and PV-inverter tests change their distortion level at nearly constant κ. The same examples also mark the limits of this reading: harmonic phase can alter operation more than κ registers, low voltage THD keeps the harmonic–harmonic fraction small, and in the capacitor records κ is close to a function of the joint spectral concentration. The demonstrated contribution is a reproducible, magnitude-only characterization of paired spectral organization; the comparative predictive and diagnostic performance of κ relative to simpler summaries remains to be established. Future work will test that performance in hardware before-and-after interventions on power electronic converters and extend the definition to sequence-indexed three-phase spectra and interharmonic bins.

When CDD is reported, the following information supports reproducible and interpretable comparisons: the declared set $\mathcal{H}$; the observation window and the aggregation convention, stating whether CDD is computed per window and then aggregated or computed from aggregated magnitudes, since the two differ (Section 4.1); S_1, a, and b together with CDD/S_1 so that the THD-determined part can be checked; κ only when both nonfundamental contents exceed the declared noise floor, together with η_{HH} and its ceiling; and, for any physical attribution, the phase-resolved, network, or intervention evidence that supports it. Under these conditions, CDD provides a magnitude-based characterization of

changes in paired harmonic spectra across declared operating conditions, including those of power electronic converters and other nonlinear loads, and can complement experimental evidence, system information, and phase-resolved models when physical attribution is required.

Supplementary Materials: The following supporting information can be downloaded at https://www.mdpi.com/article/10.3390/electronics15215117/s1: File S1: Documentation of the rectifier example of the originally submitted version, its reproduction, and its relation to the simulated population (PDF); File S2: Archive with the ngspice netlists and Python scripts that reproduce the 2500-case rectifier population, its eligible pairs, and the selected rectifier cases of Table 3, including the ±20% component-sensitivity runs, and the example of the originally submitted version; the script and per-record table of the spectral refit of the capacitor records; the illustrative sensitivity analysis of Sections 3.1.4 and 3.2.3; the comparison of κ with simpler summaries (Table 9); the ceilings of Table 6; the truncation study of Section 3.2.6; and a reference implementation of Algorithm A1 with its checks. File S2 is openly available in Zenodo at https://doi.org/10.5281/zenodo.23679555, where it also contains File S1.

Author Contributions: Conceptualization, D.D.C.-O.; methodology, D.D.C.-O.; formal analysis, D.D.C.-O.; validation, D.D.C.-O.; investigation, G.A.F.-C.; visualization, G.A.F.-C.; writing—original draft preparation, D.D.C.-O.; writing—review and editing, D.D.C.-O., G.A.F.-C. and F.A.R.; supervision, F.A.R.; project administration, F.A.R.; funding acquisition, F.A.R. All authors have read and agreed to the published version of the manuscript.

Funding: This research was funded by the U.S. National Science Foundation (NSF) EPSCoR RII Track-2 FEC Program, grant number 2316401, through the project "Collaborative Research: RII Track-2 FEC: STORM: Data-Driven Approaches for Secure Electric Grids in Communities Disproportionately Impacted by Climate Change".

Institutional Review Board Statement: Not applicable.

Informed Consent Statement: Not applicable.

Data Availability Statement: The data analyzed in this study were derived from the following resources. The university data-center dataset is openly available at https://github.com/joaquinjgz/Dataset_university_data_center accessed on 30 October 2026 [36]. The capacitor waveforms are available in the open datasets of the IEEE Power & Energy Society Intelligent Systems Subcommittee [37,40]. The photovoltaic-inverter, induction-motor, and residential spectra are taken from published sources [14,17,19]. Restrictions apply to the wind-turbine converter injection data: they were obtained from the research team of Prof. Yuanyuan Sun, Shandong University, with the permission of Prof. Wilsun Xu, and are available from that team upon reasonable request. The ngspice netlists and Python scripts that reproduce the rectifier population and the selected rectifier cases, the script and derived per-record table of the capacitor refit, the scripts and outputs of the sensitivity, summary, ceiling, and truncation analyses, and a reference implementation of Algorithm A1 are openly available in Zenodo at https://doi.org/10.5281/zenodo.23679555 accessed on 30 October 2026 (version 1.1.0).

Acknowledgments: The authors thank the research team of Yuanyuan Sun of Shandong University, China, for conducting the experiments and sharing the experimental data, and Wilsun Xu of the University of Alberta, Canada, for facilitating access to the data.

Conflicts of Interest: The authors declare no conflicts of interest. The funders had no role in the design of the study; in the collection, analyses, or interpretation of data; in the writing of the manuscript; or in the decision to publish the results.

Abbreviations

The following abbreviations are used in this manuscript:

CDD	Cross-Order Distortion Descriptor
DFT	Discrete Fourier transform
FCM	Frequency-coupling matrix
HH	Harmonic–harmonic
LC	Inductor–capacitor
PV	Photovoltaic
RMS	Root mean square
TDD	Total demand distortion
THD	Total harmonic distortion
TRD	Total rated-current distortion

Appendix A. Single-Pass Computation

Algorithm A1 evaluates the principal CDD quantities S_1, a, b, CDD, CDD_{1H}, CDD_{HH}, η_{HH}, and κ from the paired per-order magnitudes of one measurement window. It uses the closed forms (4) and (5), so the $|\mathcal{H}| \times |\mathcal{H}|$ matrix $\mathbf{M}$ is never formed: one pass over the nonfundamental orders updates three accumulators with two squarings, one product, and three additions per order, which gives $\mathcal{O}(|\mathcal{H}|)$ operations and constant memory beyond the input. The inputs are per-order RMS magnitudes of the kind specified by IEC 61000-4-7 for each measurement window [2].

Four implementation points follow from Sections 2.1.4 and 4.1. First, V_h and I_h must come from the same phase and the same window so that each product $V_m I_n$ pairs magnitudes obtained from the same observation window. Second, for comparability, temporal aggregation is preferably applied to the window-level outputs; when only aggregated magnitudes are archived, as in the data-center records, CDD is computed from them. Because the two results differ by the covariance term of Section 4.1, the convention used is declared. Third, the thresholds ε_a and ε_b implement the noise-floor condition under which κ is not interpreted. They are measurement-procedure-dependent rather than universal constants. With $\sigma_{V,h}$ and $\sigma_{I,h}$ denoting the per-order RMS noise-floor levels of the measurement procedure, a practical implementation may estimate the aggregate nonfundamental noise floors $\sigma_{V,H'} = (\sum_{h\in\mathcal{H}'} \sigma_{V,h}^2)^{1/2}$ and $\sigma_{I,H'} = (\sum_{h\in\mathcal{H}'} \sigma_{I,h}^2)^{1/2}$ and set $\varepsilon_a = \gamma\, \sigma_{V,H'}/V_1$ and $\varepsilon_b = \gamma\, \sigma_{I,H'}/I_1$, where γ is a declared detection margin; alternatively, the thresholds may be established empirically from a high percentile of the apparent nonfundamental content measured under an appropriate reference condition. If $a = 0$ or $b = 0$, the algorithm returns $\mathrm{CDD}_{HH} = 0$, and $\eta_{HH} = 0$ whenever CDD > 0; κ is not required. Fourth, line 8 subtracts nearly equal quantities when κ is close to zero, and the relative condition number of that subtraction with respect to its two operands is $(2 - \kappa)/\kappa$, so rounding errors are amplified as $\kappa \to 0$; double-precision accumulation is recommended in that regime. A Python reference implementation is included in the Supplementary Materials. It agrees with direct evaluation of (2) and (9) on 10,000 random spectra with up to 51 orders to within 10^{-15} (relative deviation of CDD; absolute deviation of κ and η_{HH}), reproduces Table 4, and reproduces the κ and η_{HH} values of the 458 capacitor records of Section 3.2.5.

Algorithm A1 Single-pass CDD for one window.

Require: declared set $\mathcal{H} = \{1\} \cup \mathcal{H}'$; magnitudes V_h, I_h for $h \in \mathcal{H}$, same phase and same window, $V_1, I_1 > 0$; declared noise-floor thresholds $\varepsilon_a, \varepsilon_b \geq 0$

$s_V \leftarrow 0$, $s_I \leftarrow 0$, $s_D \leftarrow 0$
for each $h \in \mathcal{H}'$ **do**
    $x \leftarrow V_h^2$, $y \leftarrow I_h^2$
    $s_V \leftarrow s_V + x$, $s_I \leftarrow s_I + y$, $s_D \leftarrow s_D + xy$
end for
$S_1 \leftarrow V_1 I_1$, $a \leftarrow \sqrt{s_V}/V_1$, $b \leftarrow \sqrt{s_I}/I_1$
$\mathrm{CDD}_{1H}^2 \leftarrow V_1^2 s_I + I_1^2 s_V$ ▷ (4), equals $S_1^2(a^2 + b^2)$
$\mathrm{CDD}_{HH}^2 \leftarrow \max(s_V s_I - s_D, 0)$ ▷ (5)
$\mathrm{CDD}^2 \leftarrow \mathrm{CDD}_{1H}^2 + \mathrm{CDD}_{HH}^2$
$\mathrm{CDD} \leftarrow \sqrt{\mathrm{CDD}^2}$, $\mathrm{CDD}_{1H} \leftarrow \sqrt{\mathrm{CDD}_{1H}^2}$, $\mathrm{CDD}_{HH} \leftarrow \sqrt{\mathrm{CDD}_{HH}^2}$
if $\mathrm{CDD}^2 > 0$ **then**
    $\eta_{HH} \leftarrow \mathrm{CDD}_{HH}^2/\mathrm{CDD}^2$
else
    η_{HH} not reported
end if
if $a > \varepsilon_a$ **and** $b > \varepsilon_b$ **then**
    $\kappa \leftarrow \mathrm{CDD}_{HH}^2/(s_V s_I)$
else
    κ not reported
end if
return S_1, a, b, CDD, CDD_{1H}, CDD_{HH}, η_{HH}, κ

References

1. *IEEE Std 519-2022*; IEEE Standard for Harmonic Control in Electric Power Systems (Revision of IEEE Std 519-2014). IEEE: New York, NY, USA, 2022. [CrossRef]
2. *IEC 61000-4-7:2002+AMD1:2008 CSV*; Electromagnetic Compatibility (EMC)—Part 4-7: Testing and Measurement Techniques—General Guide on Harmonics and Interharmonics Measurements and Instrumentation, for Power Supply Systems and Equipment Connected Thereto. International Electrotechnical Commission: Geneva, Switzerland, 2009.
3. George, S.; Agarwal, V. Optimum Control of Selective and Total Harmonic Distortion in Current and Voltage Under Nonsinusoidal Conditions. *IEEE Trans. Power Deliv.* **2008**, *23*, 937–944. [CrossRef]
4. *IEEE Std 3002.8-2018*; IEEE Recommended Practice for Conducting Harmonic Studies and Analysis of Industrial and Commercial Power Systems. IEEE: New York, NY, USA, 2018. [CrossRef]
5. Dugan, R.C.; McGranaghan, M.F.; Santoso, S.; Beaty, H.W. *Electrical Power Systems Quality*, 3rd ed.; McGraw-Hill: New York, NY, USA, 2012.
6. *IEEE Std 1547-2018*; IEEE Standard for Interconnection and Interoperability of Distributed Energy Resources with Associated Electric Power Systems Interfaces (Revision of IEEE Std 1547-2003). IEEE: New York, NY, USA, 2018. [CrossRef]
7. *IEEE Std 2800-2022*; IEEE Standard for Interconnection and Interoperability of Inverter-Based Resources (IBRs) Interconnecting with Associated Transmission Electric Power Systems. IEEE: New York, NY, USA, 2022. [CrossRef]
8. Blanco, A.M.; Yanchenko, S.; Meyer, J.; Schegner, P. The impact of supply voltage distortion on the harmonic current emission of non-linear loads. *Dyna* **2015**, *82*, 150–159. [CrossRef]
9. *IEEE Std 1459-2025*; IEEE Standard Definitions for the Measurement of Electric Power Quantities under Sinusoidal, Nonsinusoidal, Balanced, or Unbalanced Conditions. IEEE: New York, NY, USA, 2025. [CrossRef]
10. Akagi, H.; Kanazawa, Y.; Nabae, A. Instantaneous Reactive Power Compensators Comprising Switching Devices without Energy Storage Components. *IEEE Trans. Ind. Appl.* **1984**, *IA-20*, 625–630. [CrossRef]
11. Akagi, H.; Watanabe, E.H.; Aredes, M. The Instantaneous Power Theory. In *Instantaneous Power Theory and Applications to Power Conditioning*, 2nd ed.; Akagi, H., Watanabe, E.H., Aredes, M., Eds.; Wiley–IEEE Press: Hoboken, NJ, USA, 2017; pp. 37–109. [CrossRef]
12. Emanuel, A.E. Powers in Nonsinusoidal Situations—A Review of Definitions and Physical Meaning. *IEEE Trans. Power Deliv.* **1990**, *5*, 1377–1389. [CrossRef]
13. Mariscotti, A. Experimental Characterisation of Active and Non-Active Harmonic Power Flow of AC Rolling Stock and Interaction with the Supply Network. *IET Electr. Syst. Transp.* **2021**, *11*, 109–120. [CrossRef]

14. Montoya, F.G.; Baños, R.; Alcayde, A.; Arrabal-Campos, F.M.; Roldán-Pérez, J. Vector Geometric Algebra in Power Systems: An Updated Formulation of Apparent Power under Non-Sinusoidal Conditions. *Mathematics* **2021**, *9*, 1295. [CrossRef]
15. Czarnecki, L.S. Currents' Physical Components (CPC) concept: A fundamental of power theory. In Proceedings of the 2008 International School on Nonsinusoidal Currents and Compensation, Lagow, Poland, 10–13 June 2008; pp. 1–11. [CrossRef]
16. Tenti, P.; Paredes, H.K.M.; Mattavelli, P. Conservative Power Theory, a Framework to Approach Control and Accountability Issues in Smart Microgrids. *IEEE Trans. Power Electron.* **2011**, *26*, 664–673. [CrossRef]
17. Fauri, M. Harmonic modelling of non-linear load by means of crossed frequency admittance matrix. *IEEE Trans. Power Syst.* **1997**, *12*, 1632–1638. [CrossRef] [PubMed]
18. Lehn, P.W.; Lian, K.L. Frequency Coupling Matrix of a Voltage-Source Converter Derived from Piecewise Linear Differential Equations. *IEEE Trans. Power Deliv.* **2007**, *22*, 1603–1612. [CrossRef]
19. Yahyaie, F.; Lehn, P.W. Using Frequency Coupling Matrix Techniques for the Analysis of Harmonic Interactions. *IEEE Trans. Power Deliv.* **2016**, *31*, 112–121. [CrossRef]
20. Sun, Y.; Zhang, G.; Xu, W.; Mayordomo, J.G. A Harmonically Coupled Admittance Matrix Model for AC/DC Converters. *IEEE Trans. Power Syst.* **2007**, *22*, 1574–1582. [CrossRef]
21. Daniel, K.; Kütt, L.; Iqbal, M.N.; Shabbir, N.; Parker, M.; Jarkovoi, M. Waveform Variation Defined Model for Harmonic Current Emissions Including Cross-Order Supply Voltage Harmonics Influence. *IEEE Access* **2023**, *11*, 42276–42289. [CrossRef]
22. Xu, W.; Langella, R.; Bracale, A.; Sun, Y.; Lian, K.L.; Wang, Y.; David, J. Modeling of Inverter-Based Resources for Power System Harmonics Studies. *IEEE Trans. Power Deliv.* **2025**, *40*, 166–177. [CrossRef]
23. Kwon, J.; Wang, X.; Blaabjerg, F.; Bak, C.L.; Sularea, V.S.; Busca, C. Harmonic Interaction Analysis in a Grid-Connected Converter Using Harmonic State-Space (HSS) Modeling. *IEEE Trans. Power Electron.* **2017**, *32*, 6823–6835. [CrossRef]
24. Zeng, C.; Wu, X.; Miao, H.; Duan, H. Responsibility Division for Harmonic Instability in the Multi-Paralleled Grid-Connected Inverters System Based on Impedance Analysis. *IEEE Access* **2023**, *11*, 115450–115461. [CrossRef]
25. Ustariz, A.; Cano, E.; Tacca, H. Tensor analysis of the instantaneous power in electrical networks. *Electr. Power Syst. Res.* **2010**, *80*, 788–798. [CrossRef]
26. Menti, A.; Zacharias, T.; Milias-Argitis, J. Geometric Algebra: A Powerful Tool for Representing Power Under Nonsinusoidal Conditions. *IEEE Trans. Circuits Syst. I Regul. Pap.* **2007**, *54*, 601–609. [CrossRef]
27. LaWhite, N.; Ilić, M.D. Vector Space Decomposition of Reactive Power for Periodic Nonsinusoidal Signals. *IEEE Trans. Circuits Syst. I Fundam. Theory Appl.* **1997**, *44*, 338–346. [CrossRef]
28. Hartman, M.T.; Hashad, M. The Correlation Functions of Power as a New Proposition to Describe Power States in Circuits with Periodical Voltage and Current Waveforms. In Proceedings of the 2008 International School on Nonsinusoidal Currents and Compensation, Lagow, Poland, 10–13 June 2008; pp. 1–4. [CrossRef]
29. *IEEE Std 1459-2010*; IEEE Standard Definitions for the Measurement of Electric Power Quantities Under Sinusoidal, Nonsinusoidal, Balanced, or Unbalanced Conditions (Revision of IEEE Std 1459-2000). IEEE: New York, NY, USA, 2010. [CrossRef]
30. Buła, D. Applicability Limits of Fixed-Spectrum Harmonic Models in Weak Low-Voltage Networks. *IEEE Access* **2026**, *14*, 113877–113886. [CrossRef]
31. Shmilovitz, D. On the Definition of Total Harmonic Distortion and Its Effect on Measurement Interpretation. *IEEE Trans. Power Deliv.* **2005**, *20*, 526–528. [CrossRef]
32. Simpson, E.H. Measurement of Diversity. *Nature* **1949**, *163*, 688. [CrossRef]
33. Emanuel, A.E.; Shepherd, W.; Zakikhani, P.; Sharon, D. Suggested definition of reactive power in nonsinusoidal systems and reactive-power definitions and power-factor improvement in nonlinear systems. *Proc. Inst. Electr. Eng.* **1974**, *121*, 705–706. [CrossRef]
34. Mansoor, A.; Grady, W.; Thallam, R.; Doyle, M.; Krein, S.; Samotyj, M. Effect of supply voltage harmonics on the input current of single-phase diode bridge rectifier loads. *IEEE Trans. Power Deliv.* **1995**, *10*, 1416–1422. [CrossRef]
35. Busatto, T.; Rönnberg, S.K.; Bollen, M.H.J. Comparison of Models of Single-Phase Diode Bridge Rectifiers for Their Use in Harmonic Studies with Many Devices. *Energies* **2022**, *15*, 66. [CrossRef]
36. Garrido-Zafra, J.; Rodriguez-Cantalejo, R.D.; Gil-de Castro, A.R.; Moreno-Muñoz, A. Three-Phase Power System Harmonic Dataset from a University Data Center. Dataset, Licensed Under CC BY 4.0. 2025. Available online: https://github.com/joaquinjgz/Dataset_university_data_center (accessed on 30 October 2026).
37. Spavieri, G.; Ferreira, R.T.M.; Fernandes, R.A.S.; Lage, G.G.; Barbosa, D.; Oleskovicz, M. Particle Swarm Optimisation-Based Approach for Parameterisation of Power Capacitor Models Fed by Harmonic Voltages. *Appl. Soft Comput.* **2017**, *56*, 55–64. [CrossRef]
38. Bonett, D.G.; Wright, T.A. Sample size requirements for estimating Pearson, Kendall and Spearman correlations. *Psychometrika* **2000**, *65*, 23–28. [CrossRef]

39. Garrido-Zafra, J.; Gil-de Castro, A.R.; Calleja-Madueno, A.; Liñán Reyes, M.; Moreno-Garcia, I.M.; Moreno-Munoz, A. Harmonic Current Magnitude and Phase Angle Forecasting to Support Harmonic Power Market Planning. *IEEE Trans. Ind. Appl.* **2026**, *62*, 488–497. [CrossRef]
40. IEEE Power & Energy Society Intelligent Systems Subcommittee. Open Data Sets. [Online]. Available online: https://site.ieee.org/pes-iss/data-sets/ (accessed on 30 October 2026).
41. Joint Committee for Guides in Metrology. *International Vocabulary of Metrology—Basic and General Concepts and Associated Terms (VIM)*, 3rd ed.; JCGM 200:2012; 2008 Version with Minor Corrections; Bureau International des Poids et Mesures (BIPM): Sèvres, France, 2012. [CrossRef]
42. Aiello, M.; Cataliotti, A.; Favuzza, S.; Graditi, G. Theoretical and Experimental Comparison of Total Harmonic Distortion Factors for the Evaluation of Harmonic and Interharmonic Pollution of Grid-Connected Photovoltaic Systems. *IEEE Trans. Power Deliv.* **2006**, *21*, 1390–1397. [CrossRef]
43. Garcia-Uzca, C.; Ochoa-Correa, D. Power Quality in Grid-Connected Photovoltaic Inverters: A Systematic Review of Critical Parameters, Standards, and Mitigation Strategies. *IEEE Access* **2026**, *14*, 141821–141848. [CrossRef]
44. Betti, C.; Tinarelli, R.; Peretto, L.; Mingotti, A. Experimental Validation of Simple Power Quality Indices for Frequency Content Assessment up to 150 kHz. *Sensors* **2025**, *25*, 6716. [CrossRef] [PubMed]
45. Artale, G.; Caravello, G.; Cataliotti, A.; Cosentino, V.; Ditta, V.; Di Cara, D.; Panzavecchia, N.; Tinè, G.; Dipaola, N.; Sambataro, M.G. Measurement issues on harmonic analysis according to the IEC 61000-4-7. In Proceedings of the 25th IMEKO TC4 International Symposium and 23rd International Workshop on ADC and DAC Modelling and Testing, Brescia, Italy, 12–14 September 2022; pp. 187–192. [CrossRef]
46. Purkayastha, I.; Savoie, P.J. Effect of Harmonics on Power Measurement. *IEEE Trans. Ind. Appl.* **1990**, *26*, 944–946. [CrossRef]
47. Gianesini, B.M.; Santos, I.N.; Ribeiro, P.F. Comparison of Methods for Determining Harmonic Distortion Contributions Using the IEEE Benchmark Test System. *IEEE Trans. Power Deliv.* **2023**, *38*, 2398–2407. [CrossRef]

Disclaimer/Publisher's Note: The statements, opinions and data contained in all publications are solely those of the individual author(s) and contributor(s) and not of MDPI and/or the editor(s). MDPI and/or the editor(s) disclaim responsibility for any injury to people or property resulting from any ideas, methods, instructions or products referred to in the content.